TNO report

TNO 2021 S10234

Reconnaissance study on the impact of leakage of subsurface-stored hydrogen on groundwater chemistry

Date	29 January 2021
Author(s)	Ferike Molema
Copy no	
No. of copies	
Number of pages	69 (incl. appendices)
Number of appendices	4
Sponsor	
Project name	
Project number	060.47625/01.04.05

Reconnaissance study on the impact of leakage of subsurface-stored hydrogen on groundwater chemistry

Ferike Molema – 5607698
Date: 29-01-2021
Internship project TNO Geological Survey of the Netherlands
Supervisors: Jasper Griffioen (TNO and UU), Thilo Behrends (UU) & Alwina Hoving (TNO)

Abstract

One of the promising technologies for balancing fluctuations between energy supply from renewable energy sources and energy demand is using hydrogen for the storage of electric energy. The produced hydrogen can be stored in the porous subsurface and may be retrieved later to reproduce electricity. A disadvantage of subsurface stored hydrogen is that it is a small and light molecule. Therefore has a larger tendency to leak than other gasses through cracks and joints in the cement casing of a borehole into shallow aquifers. Redox reactions catalyzed by bacteria can oxidize the leaked hydrogen by reducing electron acceptors such as Fe(III), sulphate, and carbonate. These redox processes are Fe(III) reduction, sulphate reduction, and methanogenesis. Enhanced microbial mediated redox reactions can enhance unwanted changes in the groundwater chemistry. This research aims to improve the understanding of the effect of hydrogen leakage from subsurface storage on the geochemical composition of the groundwater and sediments in shallow aquifers. To represent an intrusion of hydrogen into a shallow aquifer, incubation experiments using pressure vessels filled with collected sediment of two different depths and two types of hydrogen enriched groundwater (fresh and brackish) were conducted. The partial pressure of hydrogen was raised towards 3.5 bar in the groundwater, by purging hydrogen gas into a KeyKeg® vessel filled with the groundwater. The groundwater and sediment were analyzed on the geochemical composition, initially and after the incubation period. Additionally, equilibrium thermodynamic calculations were performed using the code PHREEQC to assess the consequences of adding hydrogen to a shallow aquifer. Hydrogen is completely consumed within 2 days for the brackish groundwater and within 7 days for the fresh groundwater during the laboratory experiments. However, the process responsible for the removal of hydrogen is enigmatic. Methanogenesis can be excluded as there was no production of methane during the experiment. Hence, Fe or SO_4^{2-} reduction are likely candidates but the production of Fe(II) could not be detected. On the contrary, dissolved Fe concentrations decreased. The lack of data on Fe(II), SO_4^{2-} and sulphide might have limited the approach. The experimental data suggests there is potential for hydrogen removal, but no significant change in water and solid phase could be observed. Model calculations indicate that hydrogen addition is expected to lead to the successive production of hydrogen sulphide and methane.

Contents

1   Introduction

1.1   Hydrogen as a potential new major energy source

Fossil fuels are still the main source of energy in the Netherlands (Energy in the Netherlands, 2018). However, the negative side effects of fossil fuels are the emission of carbon dioxide, which makes this energy source no longer sustainable for the future. Therefore, many research groups are dedicated to finding renewable energy sources to meet future energy demand.

Potential renewable energy sources to reduce the emission of carbon dioxide are solar and wind energy, through solar panels and wind turbines. One of the downsides of wind and solar energy is the fluctuation of the created energy due to seasonal variation and changing wind conditions. The amount of energy created by these sources depends on variable climate conditions, and thus periods of shortages and peak production can be expected (Yekta et al., 2018; Pfeiffer et al., 2016). The energy created during peak production by wind turbines and solar panels can result in higher energy production than the demand by households and industry. Shortages result from higher energy demand than production. Both energy production and energy demand fluctuate, making the distribution of renewable energy challenging (Berta et al., 2018). To address this issue of fluctuating energy production and energy demand, the 'power to gas' approach originated (Conte et al., 2001).

With the 'power to gas' approach, the excess electrical energy produced by wind turbines and solar panels is stored into chemical energy. One of the possible gasses is hydrogen which can be produced by electrolysis (Berta et al., 2018; Yekta et al., 2018). This can create an energy carrier for large scale use. The 'power to gas' approach can be applied to produce hydrogen gas and store it at moments of peak electricity production (Figure 1, green arrow). The energy can then be released from the hydrogen gas at times of high electricity demand and low primary production of electricity (Figure 1, red arrow).
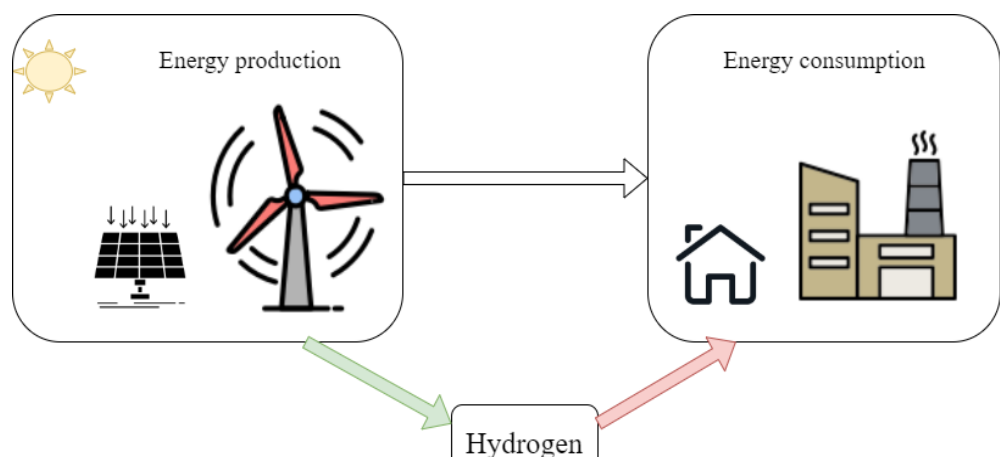

Figure 1:   The interplay between energy production, energy demand and hydrogen. The white arrow indicates the normal situation. With the creation of hydrogen the green and red arrows come into play.

Hydrogen attracts particular attention as it is an environmentally clean energy carrier. Hydrogen does not emit CO_2 in the cycles of its conversion to and from electricity (Panfilov, 2016). Furthermore, hydrogen is capable of replacing up to 60% of the natural gas used for nonindustrial activities due to its high energy density (Davison et al., 2009).

A negative aspect of creating hydrogen gas from excess energy production is the low density of hydrogen gas under normal pressure and temperature conditions. A large volume of storage is needed to store the produced hydrogen gas. Since building sites are valuable, storing hydrogen on surface grounds would make the hydrogen an expensive energy carrier.

To overcome the problem of storage costs, there is increasing attention for storing hydrogen gas in the porous subsurface. Storing hydrogen in the porous subsurface would make hydrogen gas more economical profitable (Taylor et al., 1986). Storage in the geological subsurface, such as empty gas fields, aquifers, or salt caverns, has the potential to store large quantities of hydrogen.

The problem is the scarcity of practical expertise relating to subsurface hydrogen storage. Pure hydrogen has so far only been stored in salt caverns in Texas, the USA, and Teesside (UK) (Pfeiffer et al. 2016).

1.2   Relevance and problem definition

1.2.1   *Environmental impact of hydrogen gas storage*

Environmental risks evolve when storing hydrogen gas into the subsurface. Hydrogen is a small and light molecule and can therefore easily migrate through porous media (e.g. cement casing; Yekta et al., 2018). By leaking through the casing hydrogen can be transported into the shallow aquifers (Hassannayebi et al., 2018). Hydrogen can then react with the dissolved and solid components of the shallow aquifers thereby altering mineralogy and porewater quality (Yekta et al., 2018).

Concentrations of hydrogen gas in aquifers, not affected by hydrogen intrusion, are usually in the nanomolar range (Watson et al., 2003). Hydrogen gas typically is an intermediate in biogeochemical redox reactions in the subsurface. The production of hydrogen originates from the fermentation of organic matter (Jakobsen and Postma, 1999; Watson et al., 2003). The consumption of hydrogen in the subsurface is can be either related to biotic or abiotic redox reactions (Hagemann et al., 2015).

Hydrogen is used by hydrogenotrophic bacteria, living in the groundwater and attached to the sediments of the shallow aquifer. They act as electron donor to reduce electron acceptors for gaining energy for their metabolism (Hagemann et al., 2016). Hydrogenotrophic bacteria conserve the free energy change of oxidizing hydrogen with reductants (Panfilov, 2016). The reactions initiated by bacteria are very fast and cause the transformation of hydrogen into other chemical substances (Panfilov. 2016). The bacteria conserve the energy released when breaking the hydrogen-hydrogen bonds, splitting off an electron (Panfilov, 2016).

Important processes accounting for hydrogen consumption in natural subsurface environments are iron(III) reduction, sulphate reduction, methanogenesis, and acetogenesis (Eq 1-4), catalyzed by bacteria. When not affected by hydrogen intrusion, these biotic redox processes occur at four different distinct levels in anaerobic sediment, based on the Gibbs free energy of the respective redox reactions and the hydrogen concentration (Lovley and Goodwin, 1988). Iron(III), sulphate, inorganic carbon, or dissolved carbon dioxide are reduced, catalyzed by these bacteria:

$$H_2 + 2Fe(OH)_3 + 2CO_2 \rightarrow 2FeCO_3 + 4H_2O \tag{1}$$

$$4H_2 + H^+ + SO_4^{2-} \rightarrow HS^- + 4H_2O \tag{2}$$

$$4H_2 + H^+ + HCO_3^- \rightarrow CH_4 + 3H_2O \tag{3}$$

$$4H_2 + H^+ + 2HCO_3^- \rightarrow CH_3COO^- + 4H_2O \tag{4}$$
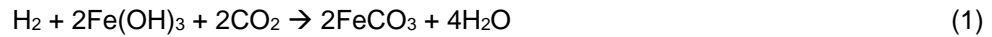
When the groundwater system is geochemically at a steady state, there are specific hydrogen concentrations associated with the dominating terminal electron acceptor, due to efficient competitive exclusion (Lovley and Goodwin, 1988). Hydrogen concentrations can be used as an indicator of the specific dominant terminal electron acceptor (TEA) by using such a partial equilibrium model (Jakobsen and Postma, 1999). According to Lovley and Goodwin (1988), when hydrogen production is limiting the electron flux, the four different redox processes do not co-occur in the sediment. Microorganisms in the subsurface sediment have each their distinct level of hydrogen concentration on which they thrive the best (Hagemann et al., 2016). Iron-reducing bacteria already thrive at low hydrogen concentrations, while sulphate reducing bacteria and methanogens need higher concentrations of hydrogen to thrive (Hagemann et al., 2016). However, evidence is found by Jakobsen et al. (1998) for iron reduction and concomitant occurrence of sulfate reduction and methanogenesis.

Besides biotic processes that utilize hydrogen gas, there are also abiotic processes that utilize hydrogen gas. Abiotic processes with hydrogen in the subsurface include geochemical reactions with minerals and rock fluids. Rates of abiotic processes are very slow at low temperatures, as the reaction constant of a reaction depends on the temperature. The reaction kinetics do not depend on the pressure. Hence, abiotic hydrogen consumption typically occurs at higher temperatures. In this research, the studied sediments and groundwaters are not deeper than 25 meters. This implies that in conditions not affected by hydrogen intrusion the potential for abiotic reactions with hydrogen is much lower. The inert behavior of hydrogen in abiotic processes at low pressure and temperature conditions comes from the strong electron-proton binding (hydrogen is a very stable molecule). The ionization energy needed to break the electron-proton binding in hydrogen makes hydrogen chemically very stable at reservoir temperature and pressure, except when it is catalyzed by bacteria (Panfilov, 2016; Truche, 2009).

1.2.2   *Effects of hydrogen leakage*

Sediments and groundwater, not affected by hydrogen intrusion, are relatively steady. However, when hydrogen is injected into subsurface storage fields, leakage of hydrogen may occur through the cement, threads, or mechanical joints in the pipeline. The leakage can lead to increased concentrations of hydrogen in shallow aquifers in the Dutch subsurface. These leakages might influence the abiotic and biotic processes in the shallow aquifers and from this the groundwater quality.

The risk of leakage in a wellbore system is also known for the subsurface storage of CO_2 (Rhino et al., 2018). This risk of leakage into the gas field emerges from the type of material used. In typical gas distribution systems, polymer pipes are used to pump methane out of the subsurface (Panfilov, 2016). A current challenge is that the permeation rate for hydrogen is about four to five times higher than the permeation rate of methane in these polymer pipes (Panfilov, 2016). Furthermore, gaskets and elastomer materials are also used in natural gas storage operations gaskets. Experiments with these materials have shown while exposing them to hydrogen/natural gas mixtures, that swelling of the gaskets and elastomers occurred. This leads to the concern of deploying these materials during hydrogen subsurface storage. Since the swelling could cause a rupture in the material, leading to leakage.

Under normal biogeochemical conditions, the consumption rate of hydrogen by bacteria is very close to its production rate (Watson et al., 2003). Accidental leakage of hydrogen into shallow aquifers may enlarge the hydrogen partial pressure. This increases the dissolved hydrogen concentration in the groundwater, probably enhancing typical redox reactions associated with hydrogen oxidation (Berta et al., 2018).

Abiotic processes related to hydrogen are for example geochemical reactions with rock minerals and reservoir fluids. Under non-elevated hydrogen concentration levels, there would be no abiotic processes going on in a shallow aquifer related to hydrogen (Truche et al., 2013). However, with increased hydrogen concentrations, there might be a possibility for abiotic processes to take place. Abiotic processes can lead to damages in the rock and mineral structure, resulting in the alteration of crucial reservoir properties like porosity and permeability.

Abiotic processes related to reservoir fluids are including the reaction between hydrogen and a (highly) saline fluid (containing e.g. $NaCl^-$, KCl^-, $CaCl_2$ and SO_4^{2-} (Pudlo et al., 2003)). In general, any input of hydrogen into (highly) saline fluid-bearing systems will most probably force a decrease in pH conditions (Pudlo et al., 2013). The lowering of the pH conditions will induce multi-mineral dissolution, but also mineral precipitation processes (Pudlo et al., 2013). For example, a lowering pH will lead to the dissolution of carbonate- and sulphate minerals (like calcite, dolomite, siderite, gypsum, anhydrite, and barite), feldspars, and clay minerals of the chlorite group will be dissolved, but in contrast, illite (K-bearing clay mineral) is likely to be formed (e.g. Allan et al. 2011, Brandt et al. 2003, Flaathen et al. 2009, Fisher et al. 2010, Velde and Meunier 2008, Pudlo et al. 2012). However, Pudlo et al. (2013) does not mention the salinity or the temperature and pressure conditions for these reactions.

Lassin et al. (2011), however, mentions a pH increase under enhanced hydrogen conditions in a porewater with a chloride concentration of 35 mmol/L. In his research, he modeled the abiotic processes related to subsurface hydrogen storage. Lassin et al., (2011) states that the main disturbance of the gas-solution geochemical system is most often the pH increase (above 10.5) and the decrease in the redox potential (down to about -700 mV) resulting from the reactions related to the dissolution of hydrogen in the pore solution. The changes in pH and pe modify the aqueous speciation and the minerals-solution equilibrium conditions (Lassin et al., 2011).

Abiotic processes related to minerals are experimentally more studied. Truche et al. (2010) studied the reduction of pyrite into pyrrhotite. The reduction happens, however, only under reservoir conditions with a pressure of at least 30 bar and temperatures as high as 150 °C ((Truche et al., 2013; Truche et al., 2010). In the same study Truche et al., (2013) showed there was no significant impact on the other minerals present in the natural claystone they used (clay minerals, quartz, calcite).

Furthermore, Alpermann and Ostertag-Henning (2019) revealed with dry mineral – H_2 experiments only hematite and pyrite oxidize significant amounts of H_2 within 14 days. These experiments were however conducted at 120°C and 20 MPa, which is much higher than the conditions in a shallow aquifer (Alpermann and Ostertag-Henning, 2019).

Abiotic processes are insignificant at temperatures below 100°C without special catalyzers (Truche, 2009). This is caused by the H-H bonding energy (436 kJ/mol), which determines a high energetic barrier that must be overcome to launch electron transfer (Panfilov, 2016). This makes hydrogen chemically inactive at reservoir temperatures (Panfilov, 2016). Due to this, geochemical reactions with minerals are considered to be slow and less relevant for gas storage operations.

1.2.3   Knowledge gap

Many studies have tried to model the influence of excess hydrogen gas on either abiotic or biotic processes in the subsurface (Hemme and Berk, 2018; Hagemann et al., 2016; Panfilov et al., 2010). They have mainly focused on hydrogen gas storage in the deeper subsurface. Experimental studies are even more scarce in the literature. One experimental study has tried to study the influence of hydrogen with the reaction of pyrite into pyrrhotite (Truche et al, 2010). Nevertheless, this study is also focused on a deeper reservoir/aquifer with higher temperature and pressure conditions. The influence of excess hydrogen on the geochemistry of shallow aquifers is poorly investigated. So far, only one study was performed which describes the influence of hydrogen in shallow aquifers on biotic processes (Berta et al., 2018).

Concluding, there is a lack of experimental data on the biogeochemical effects of excess hydrogen on shallow aquifer systems to fully understand the processes. Experimental results are required to verify and improve current insights to better understand the fate of hydrogen in shallow aquifers.

1.3   Research questions and hypotheses

This research aims to improve the understanding of the effects of hydrogen leakage from subsurface storage onto the geochemical composition of shallow aquifers. It will be investigated whether the composition of typically Dutch groundwater and sandy sediments will be affected upon leakage of hydrogen via an injection well. The following research questions become addressed:

- Does leakage of H_2 into groundwater result in the consumption of Fe(III) oxyhydroxides, SO_4^{2-} and HCO_3^- with associated production of Fe(II), H_2S, and CH_4?
- What is the dominating terminal electron acceptor (TEA) used to oxidize naturally present electron donors and will there be a shift in the dominating TEA by the presence of high H_2 concentrations in the groundwater?
- What is the effect of leakage of H_2 on the iron mineral composition of the aquifer sediment?
- Will the redox reactions initiated by an increased H_2 concentration cause a change in groundwater pH and does this influence other, non-redox hydrogeochemical processes?

The above research questions were addressed by laboratory experiments and model simulations.

The hypothesis is that enhanced production of H_2S and CH_4 will occur in the aquifer due to the leakage of H_2. The production of H_2S and CH_4 can be induced by the occurrence of highly reactive Fe-oxyhydroxides. By enhanced utilization of these TEA's, either iron or sulphate will likely get depleted and there will be a shift in the dominating TEA towards methanogenesis. Lastly, it is hypothesized that hydrogen-induced reactions will affect the pH. Most reactions are expected to lead to a consumption of H^+, but there might be a release of protons when acidic compounds are formed.

2   Background

2.1   Hydrogen gas properties related to well casings

Hydrogen is the main element in the universe (Shimko, 2008) and has the second-lowest melting and boiling points with only helium being below. Pure hydrogen is a non-toxic, odorless, colourless, and tasteless gas. Hydrogen is only dangerous if it is released in enclosed spaces where it can accumulate to explosive mixtures.

To use hydrogen as an energy carrier the electricity produced by renewable energy sources first has to be stored into hydrogen. This electricity can be stored into hydrogen in two different ways (Panfilov, 2016):
1. Low-temperature chemical electrolysis of water is performed due to the action of electrical current and catalyzers; such reactions occur in standard electrolyzers
2. High-temperature electrolysis of water is performed by electrical current and high temperature (800-1200 C); such reactions occur in nuclear plants with new generation reactors

After the conversion of electricity into hydrogen, the hydrogen needs to be stored. The storage of hydrogen is proposed to take place in empty natural gas fields. In all cases of gas underground storage a secure injection- and production cycle has to be guaranteed at all times (DBI GUT, 2017). Uncontrolled gas leakages in all parts of the wellbore system and surface facilities have to be prevented. The prevention, known as borehole integrity, is the total of all procedures that are ventured during planning, drilling, and usage of underground storage well (DBI GUT, 2017). When introducing large amounts of hydrogen in the wellbore system, borehole integrity should be retained (DBI GUT, 2017). As wellbore systems are originally designed for methane and not for hydrogen (Carden and Paterson, 1979) it is important to understand the differences and possible side effects of storing hydrogen in natural gas systems. It is therefore good to look at the gas properties of both gasses.

Hydrogen gas is much lighter and less dense than methane (Table 1). The molecular weight and density of gas influence the fugacity of a gas. Due to the low weight hydrogen has a higher fugacity than methane. The consequence of a higher fugacity is that hydrogen gas has a larger diffusion coefficient due to the higher average velocity at the same temperature. It migrates more easily through cracks and joints potentially present in the well between the casing and the cement, into the surrounding sediments and groundwater. Besides it can pass pores, which are too small for methane but large enough for hydrogen.

Table 1: Properties of methane and hydrogen (Bai et al., 2014)

Characteristics	**Unit**	**CH$_4$**	**H$_2$**
Molecular weight	g/mol	16	2
Density @ 20 °C	kg/m^3	0.717	0.0899

Hydrogen can migrate into the groundwater of the shallow aquifers by gas migration when the gas pressure exceeds the hydrostatic pressure. It will also dissolve in the surrounding groundwater when present as a gas phase. When dissolved in

groundwater, both advective and diffusive transport may occur. The diffusion of dissolved gas is dependent on the concentration gradient, where the maximum concentration of a gas component is dependent on its solubility in water.

The solubility of gases in liquids (e.g. hydrogen in water) is approximated by Henry's law (Henry, 1803). The solubility of hydrogen in water is very low (Panfilov, 2016; Lassin et al., 2011). At standard conditions, (1 atm and 25 °C) the solubility of hydrogen in pure water is about 0.784 mol/m^3 (equivalent to #1.568 mg/L) and it increases to 37 mol/m^3 at 50 bar and 30 °C (Lopez Ortiz et al., 2002).

2.2   Bacteria involved in hydrogenotrophic redox reactions

Hydrogen can be used as an electron donor by most bacteria that are capable of anaerobic dissimilation. Related to Fe(III) reduction, sulphate reduction, methanogenesis, and acetogenesis, four hydrogenotrophic bacteria species are important in hydrogen utilization in the subsurface. These are Fe(III) reducing bacteria, sulfate-reducing bacteria, methanogenic bacteria, and homoacetogenic bacteria. These four groups all have the enzyme hydrogenase (Adhikari et al., 2016; Cord-Ruwischet al., 1988).

Iron-reducers can be either heterotrophic or autotrophic (Hagemann, 2018). They are (facultative) anaerobe and interact with the reservoir rocks to transform Fe(III) into Fe(II) (Panfilov, 2016). Examples of species are *Geobacter metallireducens* and *Shewanella putrefaciens*.

Sulphate reducing bacteria (SRB) are anaerobe (Panfilov, 2016). SRB occur in geological settings ranging from 0°C to 60-80°C (Hemme and Berk, 2017). In some cases, bacterial sulphate reduction has been observed above 80 °C (Hemme and Berk, 2017) as hyperthermophilic sulphate-reducing bacteria may live up to 110 °C (Jorgensen et al., 1992). SRB can even occur in saline environments, but their activity decreases with Na^+/Cl^- concentrations above 50-100 g/l (Hemme and Berk, 2017). Usually, SRB use dissolved sulphate as a source for sulphate reduction. However, in oil and gas reservoirs SRB can derive their sulfate from the aqueous dissolution of minerals like anhydrite ($CaSO_4$). SRB mainly uses inorganic compounds as a carbon source (Hageman, 2018).

Methanogenic Archaea/Bacteria are autotrophic anaerobes. Methanogens thrive at different temperature optima, ranging from 30-40°C, but even up to higher temperatures as 80°C, and up to 97°C (Hemme and Berk, 2017). There are three groups: *Methanobacteriales, Mehtanococcales,* and *Methanomicrobiales*, and these groups include over 40 genera (Panfilov, 2016).

Acetogenic bacteria thrive the best at the same temperature and pressure as methanogens (Panfilov, 2016). Acetogenic bacteria are also autotropic, as they use inorganic carbon as an energy source, but they can also use organic sources of carbon (Hagemann, 2018).

2.3   Processes associated with well leakage of stored H$_2$

Many attempts have been made to model the geochemical consequences of underground hydrogen storage (UHS) under reservoir conditions (Gabrielli et al., 2020; Panfilov et al., 2016; Hagemann et al., 2015; Hemme and Berk, 2018; Yekta et al., 2018). However, all these studies encounter the same problem in their models: a lack of data available from experimental results.

To model the effects of UHS, we first need to understand the physical, chemical, and biological processes related to UHS. A subsurface hydrogen leak can be described in several steps.

The first step addresses how hydrogen leaks through the wellbore system from the storage reservoirs towards the shallow aquifer (Figure 2, (1)). This leakage occurs due to gas migration when the gas pressure exceeds the hydrostatic pressure. In the second step, the hydrogen gas has reached the aquifer where it can either stay in the gas phase or dissolve into the groundwater (Figure 2, (2)). The last step models abiotic and biotic geochemical processes happening in the shallow aquifer
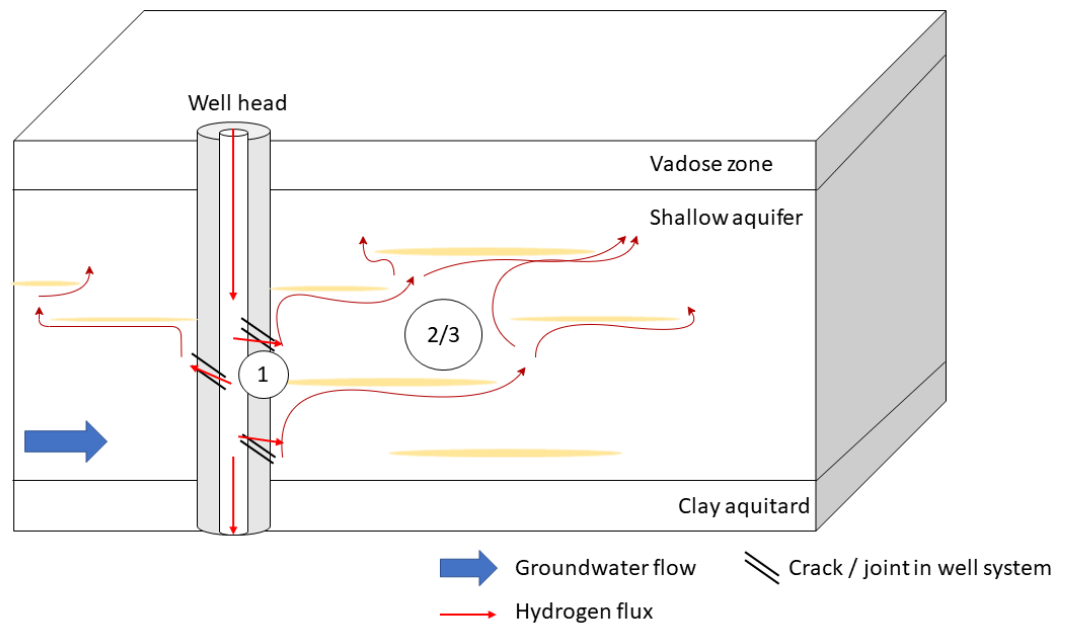
Figure 2: Simplified conceptual model of a continuous H$_2$ leakage in an shallow aquifer

(Figure 2, (3)).

Combining these steps in a model, two main parts can be considered. Firstly, the transport of hydrogen through the wellbore system and the subsurface. Secondly, the chemical reactions of hydrogen with the solids and solutes in the aquifer should be modelled, which are kinetically controlled.

The purpose of the first part of the model is to describe the dynamic behaviour of the hydrogen in the subsurface. The gas flow through the subsurface is hereby

assumed to be one-dimensional (Gabrielli et al., 2020). It can be assumed gravitational effects are neglectable when the system is a closed system, consisting initially of a pure hydrogen gas system. Simulating an open system, hydrogen has a density-drive flow, and then gravitational effects cannot be neglected. A mathematical model based on these assumptions can be described. The mathematical model consists of balance equations, namely, mass balance in the reservoir, mass balance in the pipe, momentum balance of the reservoir (Gabrielli et al., 2020). These balance equations are solved with the equation state for the gas phase (both in the pipe and reservoir), porosity equation, and permeability equation (Gabrielli et al., 2020).

The first part of the model can mathematically be described by a compositional two-phase flow model with water and gas as phases (Feldmann et al., 2016). The spatial variation of the gas phase composition between leaked hydrogen gas and originally present gas in the aquifer leads to density and viscosity contrasts which influence the displacement process (Feldmann et al., 2016). The mixing of the gases with different compositions is governed by molecular diffusion or mechanical dispersion dependent on the flow velocity (Feldmann et al., 2016).

Additionally, in this first part, the characteristics of geological formations around the borehole should be included in the model. Siliciclastic geological formations are characterized by the presence of different mineral phases, sedimentary structures, and hydrocarbons accompanied by gas impurities and formation fluids (Pudlo et al., 2013). Differences in characteristics of geological formations cause variabilities in the fluid migration and variabilities in interactions with hydrogen in physicochemical processes (Pudlo et al., 2013).

The purpose of the second part of the model is to describe the biogeochemical processes in the shallow aquifer as mediated by bacteria. The reactions involved with hydrogen are known to be microbially hydrogen-induced and therefore cannot simply be described by a chemical zero-, first- or second-order differential equation. Bacterial growth should be added to the model. Substrate-limited growth models that describe bacterial growth are either the Monod model (Monod et al., 1949) or the Moser model (Moser, 1985). It is important to describe the growth and decay of the microorganisms adequately because this is related to the local rates of the biogeochemical reactions (Hagemann et al., 2016).

However, including the bacterial growth and/or decay rate is not simple. In the current state, the kinetic parameters are estimated with very high uncertainty (Hagemann et al., 2016). More knowledge is needed of the kinetic rate constants for bacterial sulfate reduction and methanogenesis at elevated levels of pressure and temperature (Hemme and Berk, 2018). Furthermore, Hemme and Berk (2018) found that these kinetic rate constants are important factors controlling the loss of hydrogen by storage. By varying the kinetic rate constant for both bacterial sulphate reduction and methanogenesis, the rate of hydrogen loss from a storage reservoir shortens (Hemme and Berk, 2018).

The crucial parameters for modelling UHS are the amount of available electron acceptors, the storage time, and the kinetic rate constants (Hemme and Berk, 2018). Reliable data on the kinetic rates of mineral dissolution and precipitation reactions, specifically in the presence of hydrogen are scarce and often not

representative for the conditions studied (Hassanayebi et al., 2018). The problem with these parameters is that they are generally derived in presence of hydrogen as a phase or at very high temperatures, which is not applicable for studies related to lower pressures or temperatures (Hassanayebi et al., 2018).

A correct model for processes related to a leakage of hydrogen in the subsurface should therefore include many different components. The model should include the pH buffering capacity of the CO_x clayey rock, diffusion processes, reaction paths, and the kinetics of abiotic as well as possible microbially mediated redox processes (Lassin et al., 2011).

3 Methods

The research project was composed of three types of activities: fieldwork, incubation experiments in the laboratory, and modelling. Together they should provide answers to the research questions. The results from the experimental study were compared with the model created.

3.1 Sampling locations

Groundwater and sediments for the incubation experiments were collected from different regions in the Netherlands. Sampling locations for groundwater were based on their sulphate and iron concentrations. The choice for focus on these two parameters is based on the expected potentially enhanced microbial redox reactions after hydrogen gas addition.

The Dinoloket database was consulted to find groundwater wells, which have a chemical composition suitable for the purpose of this research. This led to two locations for groundwater sampling locations, one location near Zaltbommel (well B45A0433) and one near Scherpenisse (Zeeland) (well B49A0232) (Figure 3). The well near Zaltbommel contained fresh groundwater with a slightly enriched iron concentration and low sulphate concentrations according to Dinoloket (Table 2). The well near Scherpenisse (Zeeland) contains brackish groundwater and high amounts of sulphate, according to Dinoloket (Table 2).

Table 2:   Information on the two groundwater wells sampled as collected from the Dinoloket website (www.dinoloket.nl)

Location	Zaltbommel	Scherpenisse (Zeeland)
Well	B45A0433 (Monitoring well 2)	B49A0232 (Monitoring well 2)
Coordinates (RD)	148930, 421650	67530, 398690
Depth range filter	-8 meter	-10 meter
Depth groundwater table	-2.42 meter	-1.04 meter
Chloride concentration	9 mg/L	8500 mg/L
Sulphate concentration	2 mg/L	860 mg/L
Iron concentration	5.8 mg/L	3.7 mg/L

Sediment samples were taken from a borehole that was present at TNO while no attempt was made to collect fresh sediments from the field in response to the covid crisis. The core available was core B51B1904 obtained by TNO in 2019, collected near Liempde (Figure 3). This core was chosen based on the grain size of the sediment (fine to coarse sand) to mimic aquifer conditions. The total depth of the borehole was 35 meters. The top ~32 meters of the core belonged to the Boxtel Formation (Dinoloket). The last ~3 meters belonged to the Sterksel Formation (Dinoloket). One criterion in the selection for the sediments was the occurrence of "orange" stripes which could be iron oxides. Two samples were collected from different depths based on the sediment colour: a light greyish-white with orange stripes from 9-10 meter and darker brownish sediment from 24-25 meter below the surface.
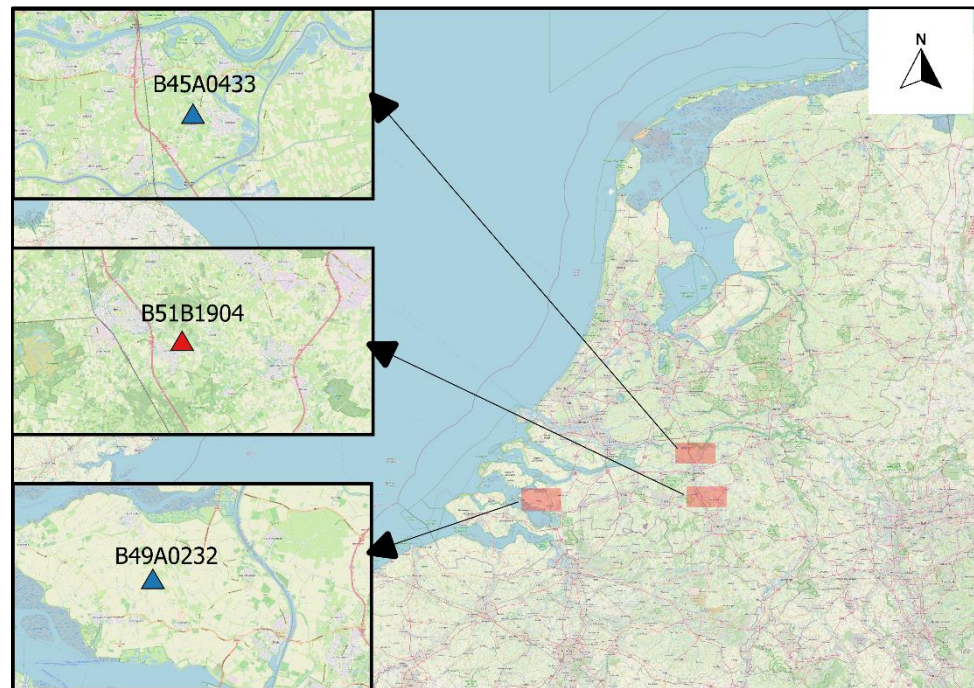
Figure 3   (Openstreetmap): Location of the groundwater wells and the collected sediment. The blue triangles are the locations of the groundwater wells and the red triangle is the location of the sediment core.

3.2   Groundwater sampling and field measurements

The groundwater was collected in the field with peristaltic pumps. Groundwater collection was performed at the depth of the filter in the groundwater well (Table 2). Before the collection of the groundwater and the field measurements could be started, the well was flushed three times, based on the volume of water in the monitoring well. The well was flushed to remove dirty water on top of fresh groundwater.

The pH, electrical conductivity, and oxygen concentration of the groundwater were measured in the field using a Hach multimeter (pH, conductivity, and dissolved oxygen electrode). The alkalinity was measured with a field kit. For this, bromcresol-green-methyl-red powder was added to 100 milliliters of groundwater followed by a titration with 1.6 N H_2SO_4 until the blue coloured groundwater changed to pink. The alkalinity was calculated from the volume of added acid. Furthermore, groundwater samples were taken for ICP-OES analysis (acidified with 22% HNO_3), IC analysis, and methane analysis (using isoflaks).

The groundwater was collected in a 10 liter keykeg®. These barrels were originally made for the storage of beer under pressure and are therefore constructed with an inner and outer wall. Inside the barrel is an aluminum bag that can be kept under pressure. When collecting groundwater under pressure, the gasses will stay dissolved in the groundwater.

3.3   Incubation experiments

Incubation experiments were set up to simulate the hydrogen leakage into a shallow aquifer. The experimental procedure consisted of several steps. First, the hydrogen was added to the groundwater sample. Second, the groundwater, enriched with hydrogen, was transferred into smaller pressure vessels containing sediments. Finally, the pressure vessels were sampled for analysis after a certain incubation time.

3.3.1   *Addition of hydrogen to groundwater*

To simulate hydrogen leakage, the concentration of hydrogen in the groundwater had to be elevated at the start of the incubation experiments. In natural systems, hydrogen is found in nanomolar concentrations in the groundwater. Here, the concentration for hydrogen was elevated to 2-3 millimolar/liter. Henry's law was used (Eq. 5) to calculate the required H_2 concentrations:

$$C_L = K_H * p \tag{5}$$

Where
- C_L is the concentration in the liquid [mol/m^3]
- K_H is Henry's constant [mol/(m^3*bar)]
- p is the partial pressure [bar]

Henry's constant for hydrogen is 0.00078 mol/(kg.bar) (for solubility at water at 298.15 K (25 °C) (NIST Chemistry WebBook). As the experiments were conducted at room temperature, Henry's constant needed to be corrected for the right temperature. The correction was performed with equation (6), where $K_H°$ is Henry's constant at 298.15 K and the term $d(\ln(K_H))/d(1/T)$ is 500 (NIST Chemistry WebBook). With the second term in Eq. (6), Henry's constant could be corrected for the right temperature.

$$K_H(T) = K_H^0 * \exp\left(\frac{d(\ln(K_H))}{d\left(\frac{1}{T}\right)} * \left(\left(\frac{1}{T}\right) - \frac{1}{(298.15\ K)}\right)\right) \tag{6}$$

Where
- $K_H(T)$ is a temperature dependent Henry's constant [mol/(m^3*bar)]
- K_H^0 is Henry's constant [mol/(m^3*bar)]
- $d(\ln(K_H))/d(1/T)$ is a temperature dependency constant [K]
- T is the temperature [K]

According to the calculations, the partial pressure of hydrogen should be elevated to 3-4 bar inside the barrel with the groundwater to get the required dissolved hydrogen concentrations (Table 3).

Table 3:   Dissolve liquid concentration and partial pressure of hydrogen gas

K_H @ 25°C [mol/(kg*bar)]	K_H @ 20°C [mol/(kg*bar)]	Partial pressure (bar)	Concentration liquid (mol/m3)
0.00078	0.000803	3	2.41
		4	3.21

The addition of hydrogen to the groundwater was accomplished by purging hydrogen gas into the keykeg® containing the sampled groundwater. The hydrogen gas was added from a one liter gas tank obtained from Lindegas (purity = 99.99%). This hydrogen gas tank was connected to the keykeg® with a pressure reducing valve fit for hydrogen gas (Figure 4). By purging hydrogen into the keykeg® from the hydrogen tank the partial pressure of hydrogen was increased towards a partial pressure of 3 bar.
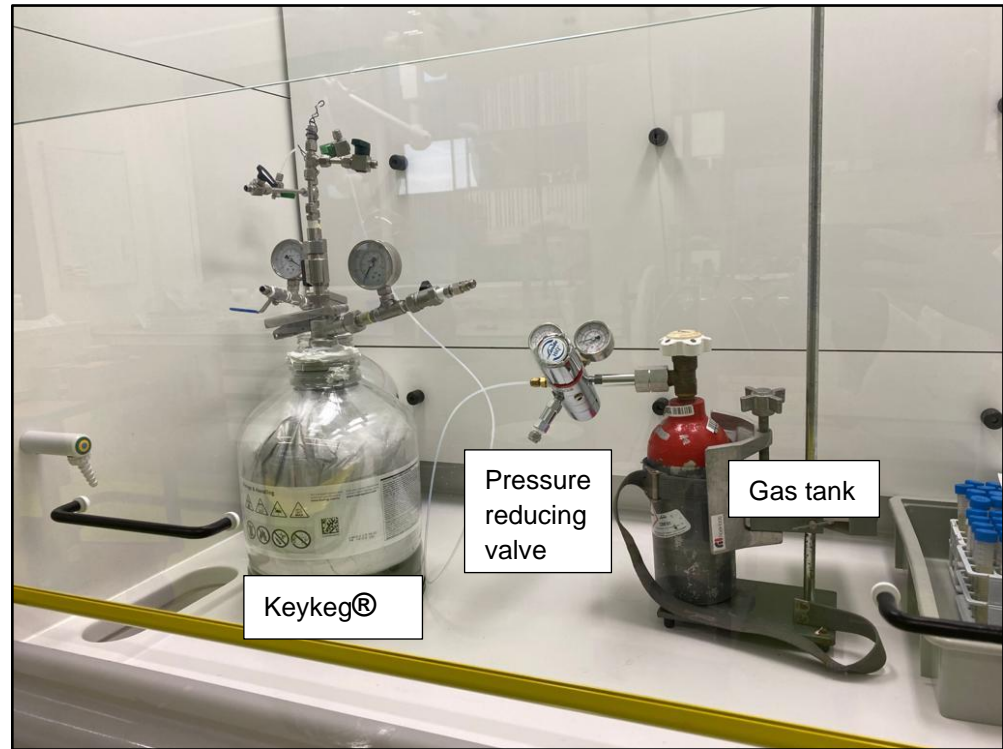

Figure 4:   Set up of the connection between the hydrogen tank and the keykeg® for the addition of hydrogen gas

There was no flow reducer between the pressure reducing valve and the keykeg® with groundwater, so the rate of purging of hydrogen was not controlled. The addition of the hydrogen gas into the keykeg® brought the system into a disequilibrium (i.e. concentrations in the gas and the aqueous phase were no longer predicted by Henry's law). The rate of diffusion of hydrogen in water is very low, due to this it takes a significant time to reach equilibrium. The time to reach equilibrium was enabled to make sure the maximum amount of hydrogen was dissolved in water. An estimation for the time to reach equilibrium was calculated. The mass transfer between the liquid phase and the gas phase was modelled with the Film Theory developed by Nernst (1904) (Appendix A). The keykeg® had a two-phase system (gas/liquid), mass transfer could take place at the interface between the gas and liquid phase. The high concentration of hydrogen at the surface of the liquid forces hydrogen molecules into the liquid until the volatilization of hydrogen from the liquid is equal to the dissolution of hydrogen into the liquid. Equilibrium is reached when the dissolution is equal to the volatilization. The time required to reach equilibrium was estimated to be around 99 min for a partial pressure of 3 bar hydrogen (Appendix A).

3.3.2 *Set up of incubation experiment*

Reference incubations were prepared in 300 ml glass vials closed with a thick butyl stopper. These reference incubations were set up with 30 grams of sediment and 200 ml of groundwater. Weighing of the sediments was performed in an argon purged glovebox to prevent oxidation of the sediment. The incubations with the deepest sediments from 24-25 m were enriched with 0.1 gram of lepidocrocite (Fe-oxide) to make sure that there were iron oxides in the sediment. The water and sediment in the reference incubations were analyzed at two different time steps (Table 4).

Table 4: Incubation scheme of the references

Vessel	Groundwater sample	Sediment sample	Time interval incubation
1	Sulphate rich	10-11m	21 days
2	Sulphate poor	10-11m	14 days
3	Sulphate rich	10-11m	14 days
4	Sulphate poor	10-11m	21 days
5	Sulphate rich	24-25m + lepidocrocite	21 days
6	Sulphate poor	24-25m + lepidocrocite	21 days
7	Sulphate rich	24-25m + lepidocrocite	14 days
8	Sulphate poor	24-25m + lepidocrocite	14 days

The incubation experiments were set up to simulate a hydrogen leakage after the addition of hydrogen gas in the groundwater. Four incubation combinations were made with the groundwater from Zaltbommel and Zeeland and the 10-11m and 24-25m+Fe-oxide sediment. These four combinations were performed parallel in six vessels, of which two vessels stood the maximum incubation time (Table 5). In the 750 ml Teflon incubation vessels 75 grams of sediment and 500 ml of groundwater were incubated. The weighing of the sediments was performed in an argon purged glovebox, to prevent oxidation of the sediment. As for the reference incubations, ~ 0.25 gram of lepidocrocite was added to half of the incubations to make sure that iron oxides were present in the sediment. The addition of groundwater to the vessel was performed with a conduit which was vacuumed up to -0.7 bar to extract as much oxygen as possible (Figure 5). During the addition of the groundwater into the pressure vessels, the pressure in the vessels increased due to the compression of the nitrogen gas in the headspace. These vessels were incubated over different timesteps (Table 5).

Table 5: Incubation scheme of the hydrogen gas incubations

| Vessel	Step	Start date	End date	Days	Groundwater sample	Sediment sample
1	1.1	24-11	01-12	7	Sulphate rich	10-11m
	1.2	01-12	08-12	7	Sulphate poor	10-11m
	1.3	08-12	10-12	2	Sulphate poor	10-11m
2	2.1	24-11	10-12	16	Sulphate rich	10-11m
3	3.1	24-11	10-12	16	Sulphate rich	24-25m + Lepidocrocite
4	4.1	24-11	01-12	7	Sulphate rich	24-25m + Lepidocrocite
	4.2	01-12	08-12	7	Sulphate poor	24-25m + Lepidocrocite
	4.3	08-12	10-12	2	Sulphate poor	24-25m + Lepidocrocite
5	5.1	24-11	26-11	2	Sulphate rich	24-25m + Lepidocrocite
	5.2	26-11	10-12	14	Sulphate poor	24-25m + Lepidocrocite
6	6.1	24-11	26-11	2	Sulphate rich	10-11m
	6.2	26-11	10-12	14	Sulphate poor	10-11m
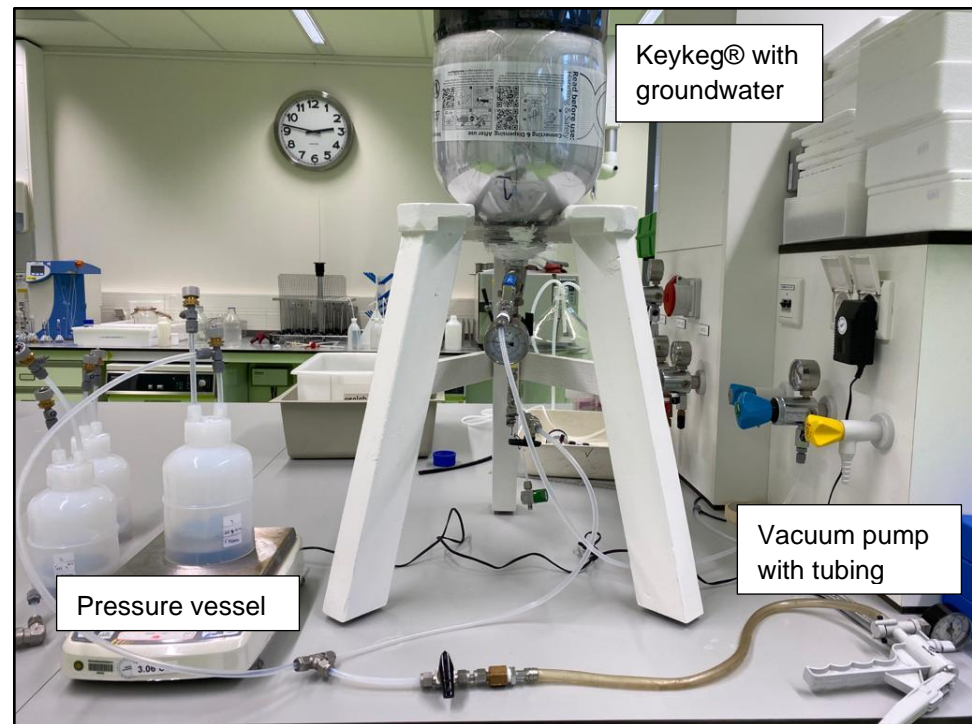
Figure 5: Set-up of the transfer of the hydrogen enriched groundwater into the incubation pressure vessel

Afterwards, all incubations (reference and hydrogen) were sampled for gas, groundwater samples and sediment analyses. The groundwater samples were filtered over a 0.2 μm filter, before analysis. The sediment samples were dried in the argon purged glovebox to prevent oxidation of the sediment.

3.4   Analytical methods

Standard analytical methods were performed to measure the pH, electrical conductance, and alkalinity. Analysis of alkalinity in the laboratory was performed with a 0.01 M HCl titer.

To measure the gas content of the headspace aliquots of samples were sent to Isolab in the Netherlands for analysis. For this, 10 ml of liquid was sampled with a needle and stored in a small glass vial closed with a thick butyl rubber stopper. Isolab analysed the samples for the gasses: C1-C6, H_2, CO_2, O_2, N_2, and Ar. Furthermore, methane and hydrogen were also measured in the laboratory of Utrecht University. These gas samples could not be measured directly, as both gas chromatograms were not running for a certain period.

Anions were measured with the ion chromatograph of Utrecht University. One millimeter of a groundwater sample was put into a small glass vial, which was analysed afterward.

Cations were measured with an inductively coupled plasma – optical emission spectrometer (ICP-OES). Before analysis could take place, 10 millimeters of groundwater was acidified with 250 μm HNO_3 (32%).

Iron speciation of the sediment was determined with a sequential extraction scheme based on Claff et al. (2010) and Poulton and Canfield (2005) (Table 6). Five different extractants were sequentially used to determine the different iron phases in the sediment. The targeted iron phases include iron-oxides, iron-carbonates, and iron-sulphides. The extracts were analysed colorimetrically according to the method by Viollier et al. (2000). Only the extracts obtained in the third step (sodium dithionite) were measured with the ICP-OES, due to interferences with the colorimetric method.

Table 6:   Iron extraction scheme based on Claff et al. (2010) and Poulton and Canfield (2005)

Step	Target	Extractant	Time	Reference
1	Carbonate Fe, including siderite and ankerite	Na acetate (1 M), pH 4.5 (acetic acid)	24 hours	Poulton and Canfield (2005)
2	Iron sulphides and iron oxides	1 M Hydroxylamine-HCl	4 hours	Claff et al., (2010)
3	Goethite, akaganéite, hematite	Sodium dithionite (50 g/L) with 0.35 M acetic acid and 0.2 M sodium citrate	2 hours	Poulton and Canfield (2005)
4	Magnetite	Ammonium oxalate	6 hours	Poulton and Canfield (2005)
5	Pyrite	Concentrated HNO_3	2 hours	Claff et al., (2010)

3.5   Modelling

In addition to the incubation experiment, leakage of hydrogen was also simulated in PHREEQC. PHREEQC (PH-Redox-Equilibrium) is a program written in the C++ language, for simulating chemical reactions and transport processes in natural or polluted water, in laboratory experiments, or industrial processes (Parkhurst and Appelo, 1999). The program is based on equilibrium thermodynamics of aqueous solutions, exchangers, and sorption surfaces and has evolved to include the capability to model kinetic reactions and 1D transport. The program reads the thermodynamic equilibrium parameters from a thermodynamic database. Several databases exist which can be used in PHREEQC, however, the database can also be adjusted to the user's own needs. In the database, the solution species, phases, exchange species, and surface species are defined. In this model, a database was adjusted from phreeqc.dat. The section ECHANGE_SPECIES in the database was adjusted by including more exchange reactions for cation-exchangers, besides the standard included exchange species (X). This was performed based on two pH ranges (6-8 (Y) and 8-10 (Z)).

3.5.1   Model set up

As described in Chapter 2, it is difficult to correctly model the system as more data is needed to create a kinetically correct model. The model used in this study is not based on kinetics, but by every addition of hydrogen, a new equilibrium is modelled by PHREEQC.

The model for simulating hydrogen leakage in a natural setting consisted of two parts. The first part simulated the initial aquifer conditions and the second part simulated the hydrogen leakage into the aquifer system (APPENDIX 1). It was

assumed that the natural setting could be seen as an aquifer with a pressure of 3 bar.

In the first part of the model, the groundwater, sediments, and gasses in the subsurface were equilibrated with each other. The groundwater in the aquifer was simulated as a SOLUTION, the sediments as EQUILIBRIUM_PHASES, and the gasses were simulated with GAS_PHASE. These three different phases were set up to react with each other at a certain reaction temperature and pressure defined. As sediment was included in this model, adsorption processes on surface areas should be included. To account for adsorption processes onto clay minerals EXCHANGE was included in the model. This keyword data block was used to define the amount and composition of an assemblage of exchangers (Appelo and Postma, 2005). In the model, the exchange sites were determined to specify that each exchanger is in equilibrium with a solution of fixed composition. The exchange master species, stoichiometries, and log Ks for the exchange reactions were defined within the database.

In the second part of the model, hydrogen was added to the equilibrated phases in the system. Hydrogen gas was added with REACTION. REACTION lets you add a substance in a certain stoichiometry and amount as if it is a titration. With the number of steps and the chosen amount, the program created a new equilibrium at each step. It was assumed that hydrogen gas reacts with a stoichiometry of one.

Redox reactions in the model can be defined within the SOLUTION data block. However, the pe and redox couples are not initially known for the groundwater. Therefore, these two parameters were kept default during the modelling. PHREEQC then calculates the pe based on the available redox couples, defined in the SOLUTION data block.

3.5.2 *Initial conditions and assumptions*

The initial conditions were based on the collected groundwater used in the experiment to simulate the effect of the hydrogen leakage on an aquifer in the shallow subsurface. When the modelling was performed, the exact composition of the sediments was not known. For the sediment, it was chosen to estimate the initial conditions. The two collected groundwater samples were both used for simulation of the leakage with hydrogen.

The initial parameters in the key block SOLUTION were based on chemical values retrieved from the two groundwater samples. However, as there were not yet results from the IC, the concentrations of chloride and sulphate were initially taken from Dinoloket. For the pe, the standard input of the program was taken as the initial condition, because the pe was not measured during the fieldwork.

The pressure and temperature in the key blocks REACTION_PRESSURE and REACTION_TEMPERATURE were based on the geothermal gradient and the pressure gradient.

In the key block EQUILIBRIUM_PHASES, it was assumed that there were quartz, calcite, and siderite initial present in the sediment. For siderite, it was assumed that the saturation index was 0.5, which is commonly found in Dutch groundwater

(Griffioen et al., 2013). For quartz and calcite, the saturation index was kept default (0.0).

The parameters in the key block GAS_PHASE were pressure, volume, temperature, and initial gasses. The pressure and temperature were kept the same as in REACTION_PRESSURE and REACTION_TEMPERATURE. In the initial gas composition, it was decided to only have a partial pressure of 0.01 for CO_2, and no initial partial pressure for CH_4. By keeping CH_4 out of the initial phases, it could be seen if it would be formed by the addition of the hydrogen gas.

To calculate the influence of the adsorption processes onto solid phases in the EXCHANGE key block, the cation exchange capacity (CEC) of the soil was calculated. The adsorption capacity is linked to the clay content, clay minerals, organic matter, and oxide or hydroxide content (Apello and Postma, 2005). The CEC relates the fractions of clay and organic carbon (Equation 15).

$$CEC \left(\frac{mmol}{kg}\right) = 25 * Organic\ matter + 5 * clay\ content \tag{15}$$

Where
- CEC is the adsorption capacity [mmol/kg]
- Organic matter describes the concentration of organic matter in the sediment
- Clay content describes the percentage of clay in the sediment

It was chosen to distribute the CEC in the fractions 80:10:10 between X:Y:Z. These X, Y, and Z were linked to exchange species in the database, based on the pH. X represents the pH of 6, Y represents the pH of 8 and Z represents the pH of 10. So this would imply that most of the CEC are available for alkaline cations at a pH of 7 and some H^+ buffering occurs at higher pH.

Finally, the amount of hydrogen gas to react with the above-mentioned phases was 3 millimoles. This was added with REACTION. It was added in 15 steps for the groundwater from Zaltbommel and in 13 steps for the groundwater from Zeeland. In each step 1/15 part for Zaltbommel and 1/13 part for Zeeland of the amount of hydrogen gas added (3 millimoles) was used by the model to calculate a new equilibrium.

4 Results

In this section, the results from the laboratory experiments and the model will be presented. First, experimental data related to the research questions will be shown, followed by parameters that might influence the redox processes. Secondly, the results of the model related to the research questions are presented, and finally, the saturation indexes calculated by the model are shown.

4.1 Experimental results

4.1.1 Hydrogen, pH, alkalinity, and dissolved concentrations of methane, iron, and sulphur

The addition of hydrogen gas to the groundwater resulted in increased concentrations of hydrogen gas (Figure 6). In the groundwater, the concentration in the gas phase of hydrogen was raised to 377 ppm for Zaltbommel. For Zeeland, the concentration in the gas phase, in the groundwater, was raised to 366 ppm. Hydrogen concentrations decrease faster in the groundwater from Zeeland than in the groundwater from Zaltbommel (Figure 6). Within two days the hydrogen concentration in the groundwater of Zeeland is below the detection limit, while for Zaltbommel this takes around 7 days. Between the two sediment types (10-11m and 24-25m+Fe-oxide) there is no clear difference in the decrease of hydrogen concentrations.
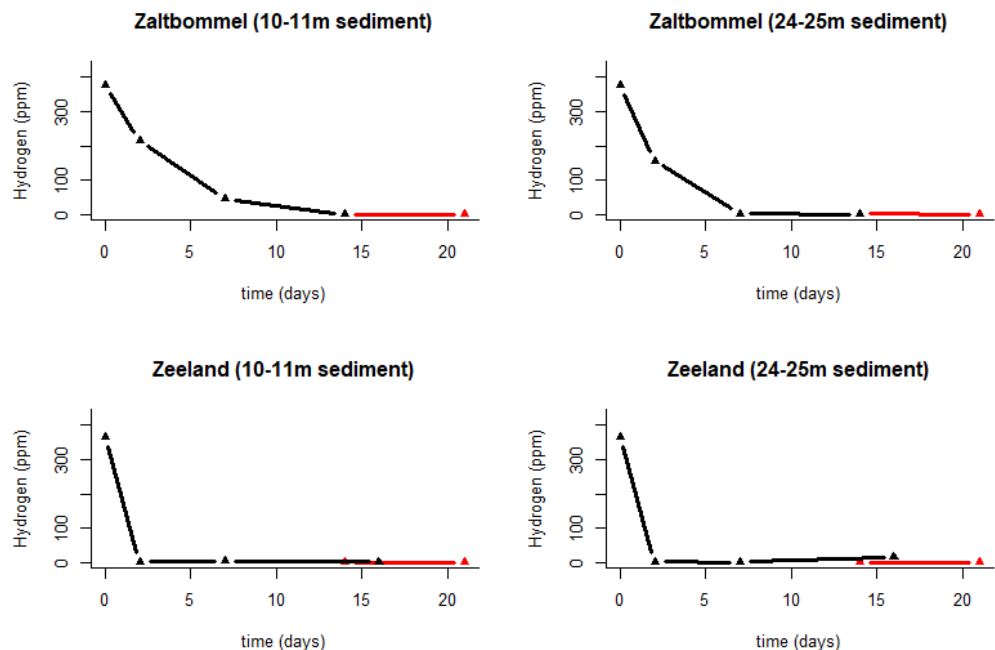

Figure 6:   The concentration of hydrogen in the gas phase plotted against time for both hydrogen incubations (black) and reference incubations (red).

All incubations show a pH increase following incubation (Figure 7). The pH rise occurred in both the reference incubations (red) and the incubations with added

hydrogen (black), to the same value. The pH increase differed between the groundwater from Zaltbommel and the groundwater from Zeeland. The groundwater from Zeeland had a maximum of ~8.2 after 2 days and decreases back to ~7.7. There is no clear difference visible between the pH increase in the 24-25m+Fe-oxide sediment and the 10-11m sediment.
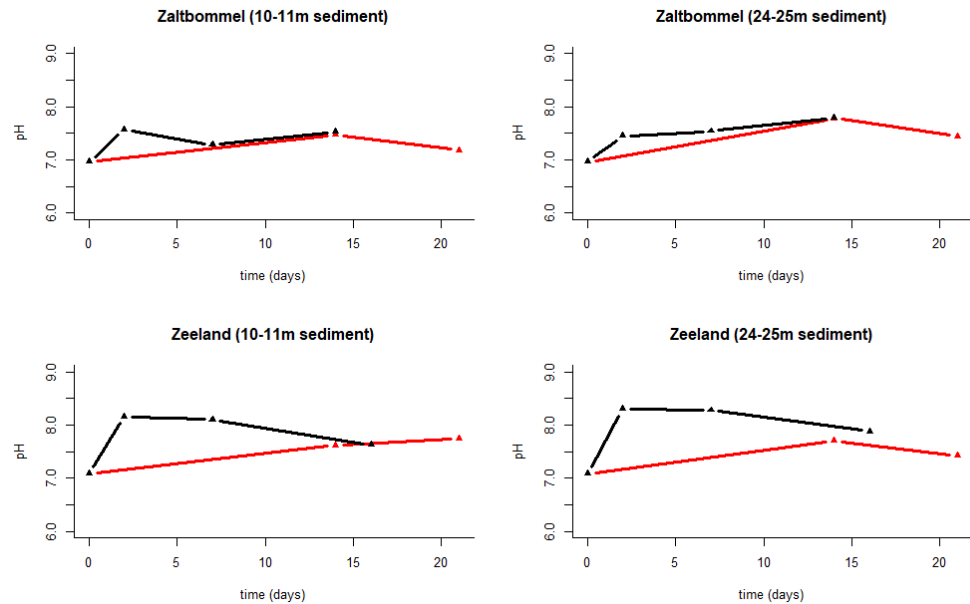

Figure 7:   pH plotted against time for the reference incubations (red) and the incubations with added hydrogen (black)

The alkalinity increased during both incubations and there is no clear difference between the reference incubations and the incubations with the added hydrogen (Figure 8). It increased more in the incubations with the groundwater from Zeeland than that with groundwater from Zaltbommel. The 24-25m+Fe-oxide sediments increased slightly more in alkalinity than the 10-11m sediments.
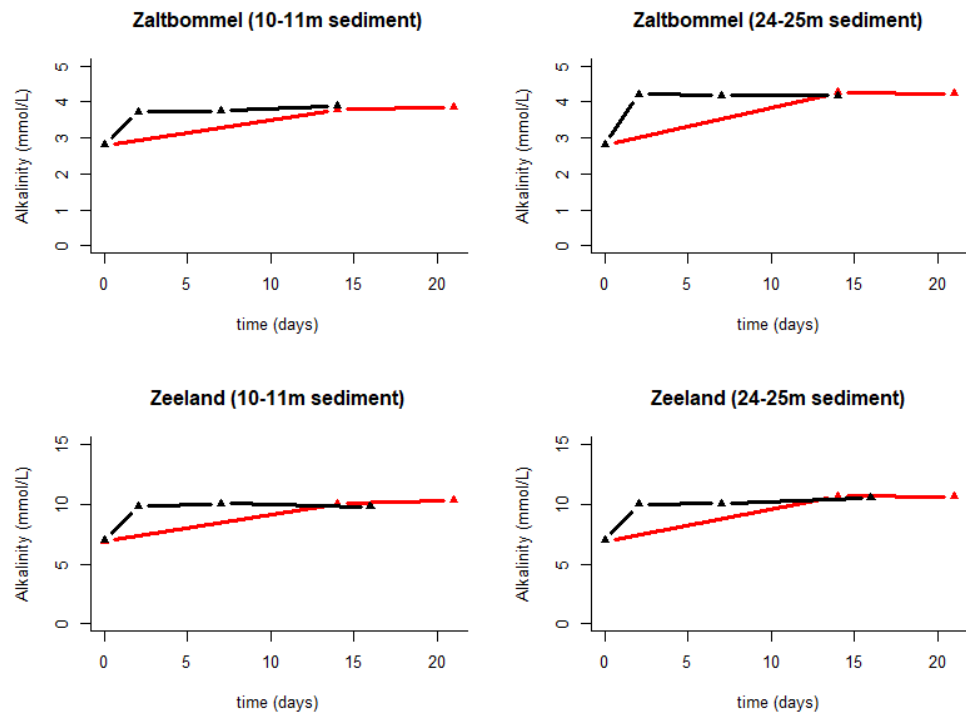
Figure 8: Alkalinity plotted against the time for the reference incubations (red) and the incubations with added hydrogen (black)

The dissolved concentration of CO_2 and CH_4 was calculated from the gas composition of the headspace. The dissolved CO_2 concentration drops in both the reference incubations and the incubations with added hydrogen (Figure 9). The CO_2 concentrations were slightly higher in the incubations with added hydrogen (black) than the reference incubations (red) at the last sampling moment. The incubation with the groundwater from Zaltbommel shows a difference in trajectory for the incubations with hydrogen and the reference incubations. The concentration of dissolved CO_2 in the reference incubations drop below the detection limit, while the incubations with hydrogen have the lowest dissolved CO_2 concentration of 0.4 mmol/L for 24-25m+Fe-oxide sediment and 0.5 mmol/L for 10-11m sediment. For the groundwater from Zeeland, the concentration of dissolved CO_2 in the reference incubations and incubations with added hydrogen drop below the detection limit.
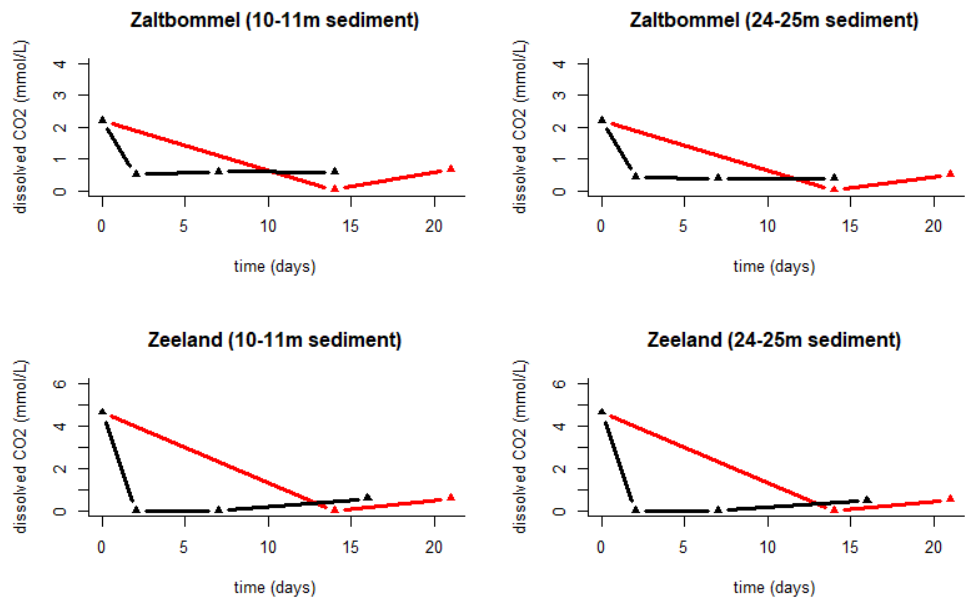
Figure 9:   Dissolved CO_2 plotted against the time for the reference incubations (red) and the incubations with added hydrogen (black)

The dissolved methane concentrations in the groundwater from both Zaltbommel and Zeeland are initially already close to zero, especially for the groundwater from Zeeland (Figure 10). For both the reference incubations and the incubations with hydrogen the methane which is present in the system is lost during the incubation. In the gas phase, there is initially methane present (Appendix C: Figure 27).
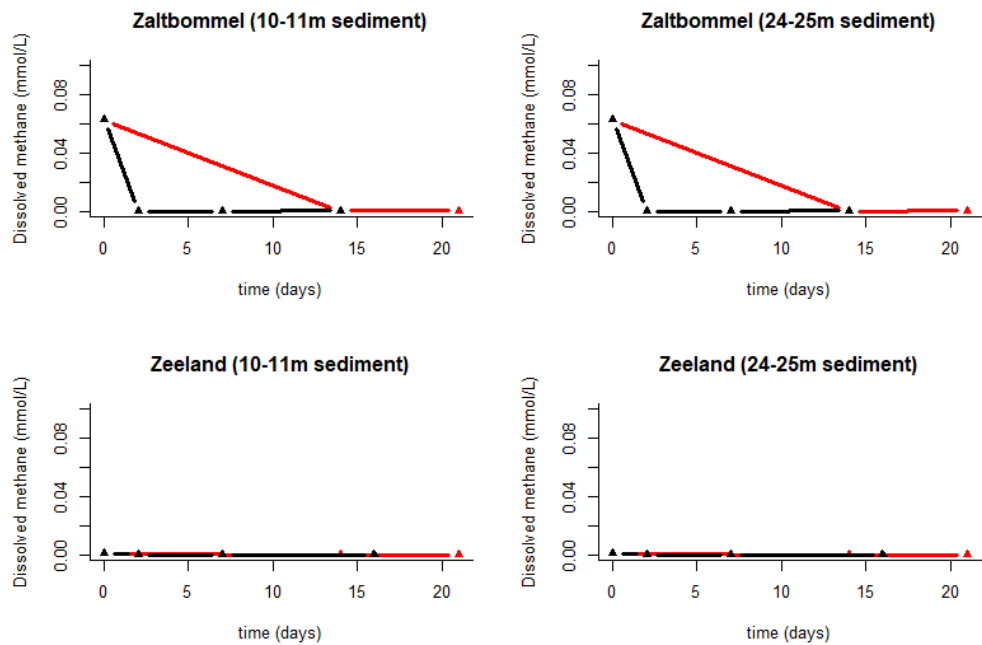

Figure 10:   Methane concentration plotted against the time for the reference incubations (red) and the incubations with added hydrogen (black)

Initially, dissolved iron is present in both types of groundwater (Figure 11). In the incubation experiments with the collected groundwater from Zeeland, the dissolved iron concentration drops below the detection limit within two days for the incubations with hydrogen (Figure 11, bottom). In the reference incubations with the groundwater from Zeeland, the dissolved iron concentration also drop below the detection limit. For the groundwater from Zaltbommel, the dissolved iron concentration does not go below the detection limit in the hydrogen incubation with the 10-11 m sediment, while this is the case for the incubation with the 25-25m sediment (Figure 11, upper).
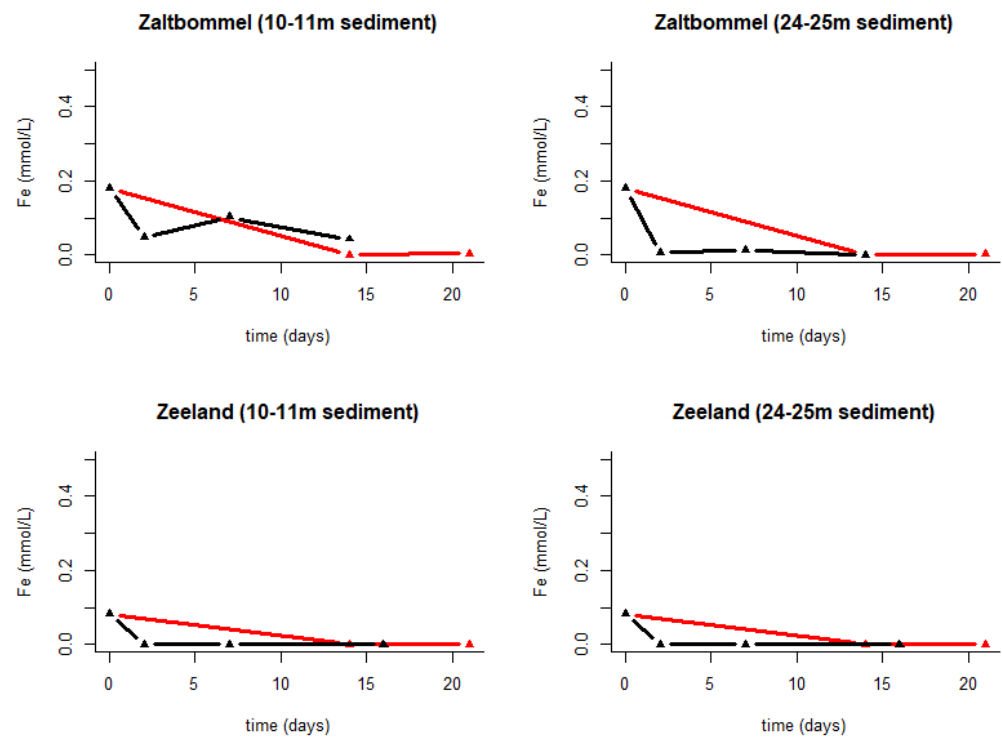
Figure 11: Dissolved iron plotted against the time for the reference incubations (red) and the incubations with added hydrogen (black)

The sequential Fe extraction shows that Fe does not occur as magnetite and pyrite in the initial sediments and is neither found during the incubation experiments (Figure 12). For the dithionite step of the sequential Fe extraction (crystalline iron oxides), the data is not yet processed.

The iron mineral phases which are found in the sediments are the carbonates, oxides, and non-pyrite sulfides. The total fraction of solid Fe is not constant throughout the different timesteps for both the reference incubations and the incubations with added hydrogen (Figure 12). However, there is a lack of data from the crystalline iron oxides. In most cases, the total fraction of solid Fe decreases, except for Zaltbommel (10-11m) with hydrogen and reference Zaltbommel (24-25m).

Iron carbonate shows distinct patterns between the different incubation experiments (Figure 12). In most of the incubations (Zaltbommel 24-25m, Zeeland 10-11m, and Zeeland 24-25m) there is a decrease over time in the iron carbonate content (Figure 12). In the incubation of Zaltbommel 24-25m, there is an increase in the content of iron carbonate, while the content decreases in the reference incubation.

In the second step of the sequential extraction scheme, iron sulphide and easy soluble iron-oxides are extracted. The distinction between the iron(II) concentration and the iron(III) concentration in the sediment is measured colorimetric during this step. Initially, there is no iron(III) in the 24-25m sediment, while this is occurring in the 10-11m sediment (Figure 12). In the 24-25m sediment the non-pyrite Fe-sulphide and Fe-oxides pool decreases, while in the 10-11m sediment these phases are relatively constant. Within the non-pyrite Fe-sulphide and Fe-oxides pool, the Fe(II) and Fe(III) content are not constant and the ratio between Fe(II) and Fe(III) differs in each time step.
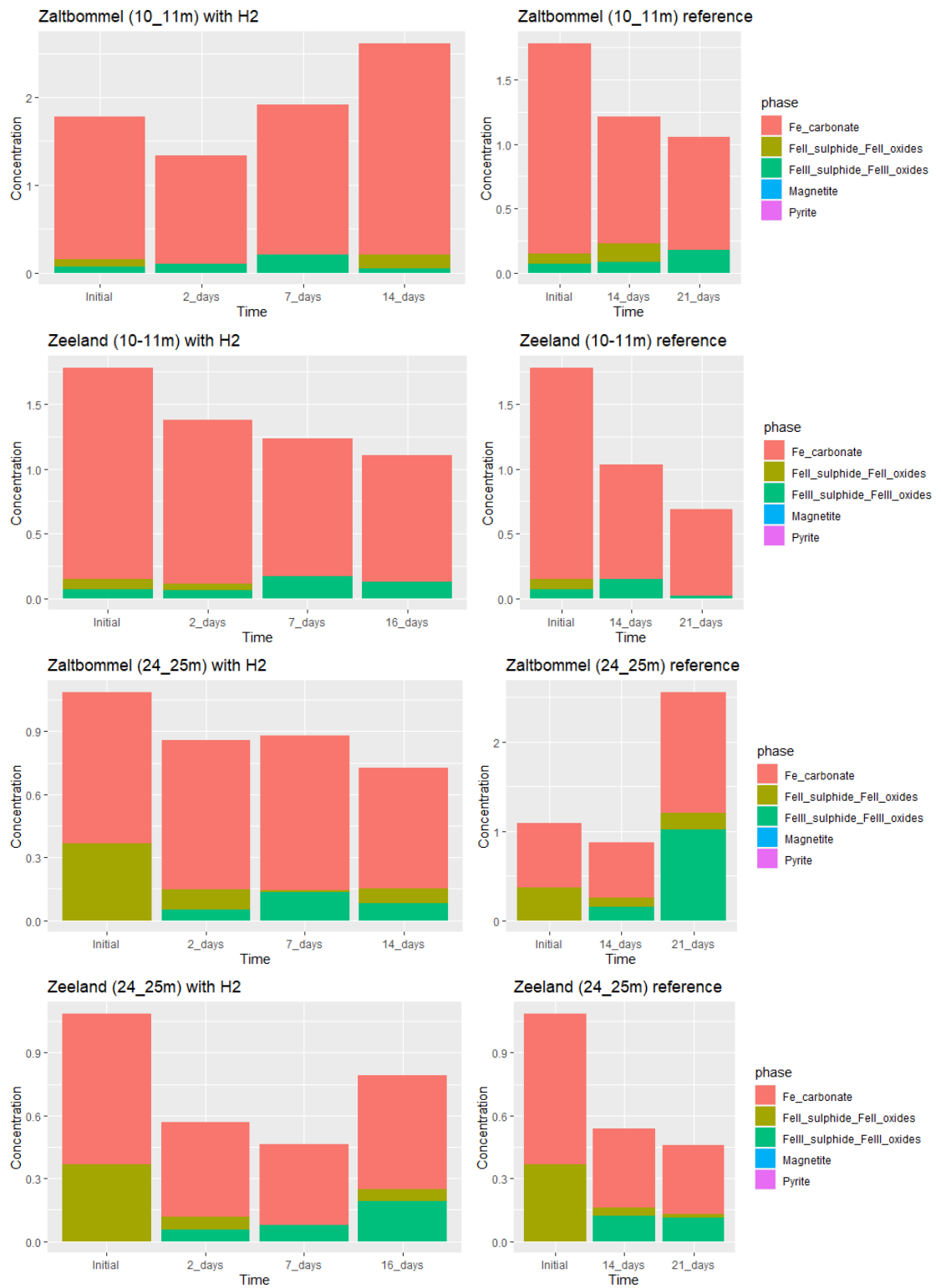
Figure 12: Cumulative content of the iron minerals in the different time steps. The amorphous iron oxides are left out, as the data is not yet processed.

There are not yet results from sulphate concentrations from the IC because the machine was not operational. However, there are results of total sulphur from the ICP-OES. The groundwater from Zeeland shows a relatively constant concentration

of total Sulphur in the incubation experiments (Figure 13). The sulphur concentration in the groundwater from Zaltbommel shows an increase (Figure 13).
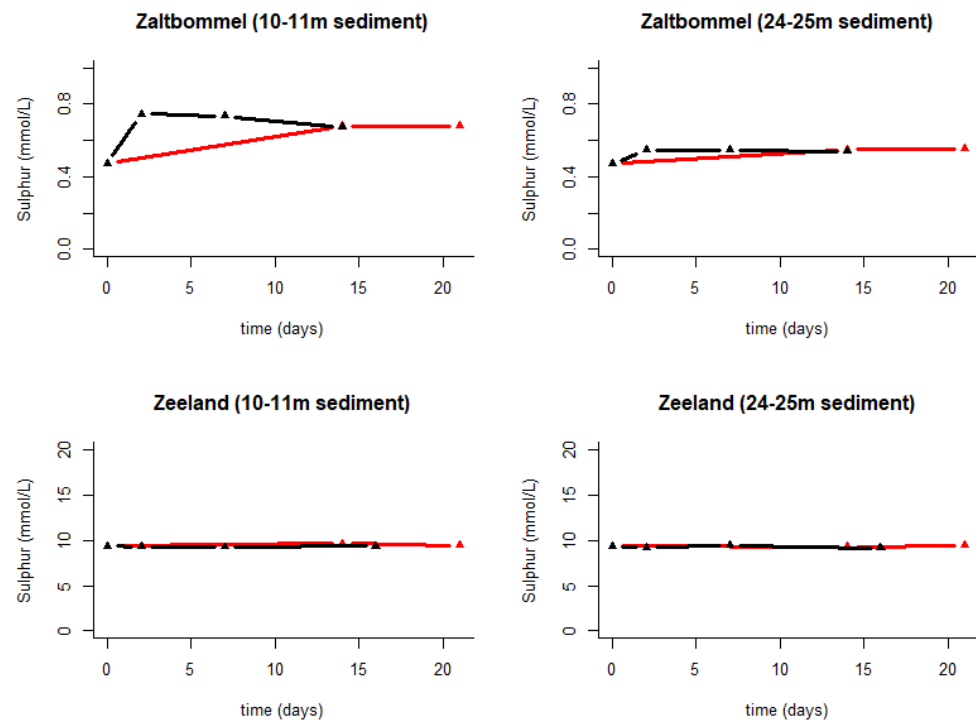

Figure 13:   Sulphur plotted against time for the reference incubations (red) and the incubations with added hydrogen (black)

4.1.2   *Remainder parameters that might influence the redox processes*

The remainder parameters, within the scope of the project, measured are the electrical conductivity (EC), calcium, magnesium and phosphorus.
The EC is a measure of the total amount of dissolved ions, which relates to the ability of the material to conduct electrical current through it. The EC shows no clear difference between the reference incubations and the incubations with the added hydrogen (Appendix C: Figure 24).
The concentration of calcium is constant throughout the experiment and no differences between the reference incubations and the incubations with the added hydrogen (Appendix C: Figure 25). The concentration of phosphorus decreases during the experiment (Appendix C: Figure 26). The decrease is in the same order for the reference incubations and the incubations with the added hydrogen.
The concentration of magnesium is also constant throughout the experiment (Appendix C: Figure 27). There is also no difference between the reference incubation and the incubation with the added hydrogen.

4.2   **Modelling results**

The model is run two times with different input concentrations from both groundwaters of the species most important for this research. Two model outputs are obtained, one can resemble the experiments with the groundwater from Zaltbommel and one can resemble the experiments with the groundwater from Zeeland.

In the model, hydrogen is added in a stepwise method, comparable to a titration. The model calculates the new equilibrium after each addition of hydrogen. The simulation results are shown in the figures below. There are three stages in this model.

1. Step 0 shows the initial conditions inside the simulated environment.
2. Step 1 shows the calculated equilibrium from the initial conditions.
3. Step 2 and following simulate the addition of hydrogen in a stepwise manner and calculates each equilibrium based on the new hydrogen concentration.

The model only calculates the equilibrium conditions and does not take into account the reaction kinetics.

4.2.1   pH, alkalinity, and dissolved concentrations

The Fe(II) dissolved iron in the model with the groundwater from Zaltbommel drops during the first calculated equilibrium, then it increases until it stays constant during the equilibrium calculations (Figure 14, left). The Fe(III) dissolved iron drops after the first step of hydrogen addition towards zero (Figure 14, left). The Fe(II) dissolved iron in the model with the groundwater from Zeeland increases after each new calculated equilibrium (Figure 14, right). The Fe(III) dissolved iron remains zero during every calculated equilibrium.

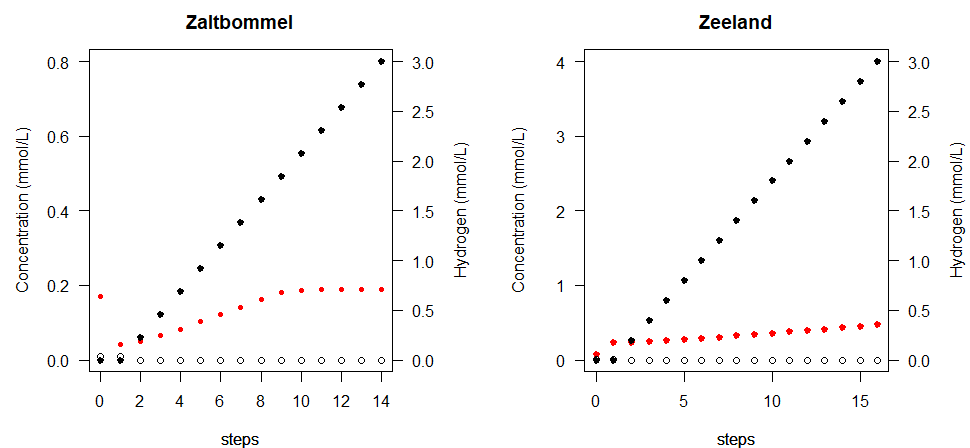Figure 14:   The equilibrium between Fe(II) (red) / Fe(III) (open) (left axis) and hydrogen (right axis, black) for each step of hydrogen addition in the model

The amount of SO_4^{2-} decreases after step 1 with each new equilibrium calculated for both the model of Zaltbommel and Zeeland (Figure 15). The amount of H_2S increases after step 1 with each new equilibrium calculated for both models (Figure 15).
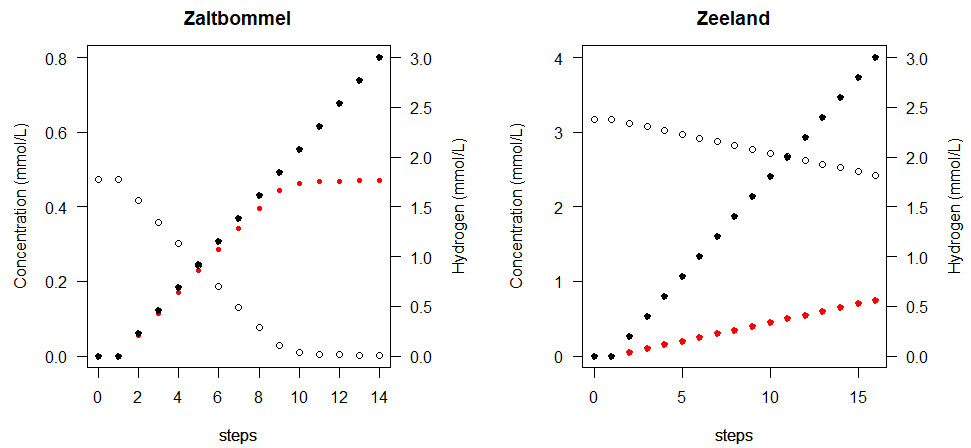
Figure 15: The equilibrium between H_2S (red) / SO_4^{2-} (open) and hydrogen (right axis, black) for each step of hydrogen addition in the model

The alkalinity in the model with the groundwater from Zaltbommel increases after step 1 with each new equilibrium calculated, while the alkalinity in the model with the groundwater from Zeeland decreases after step 1 with each new equilibrium (Figure 16).
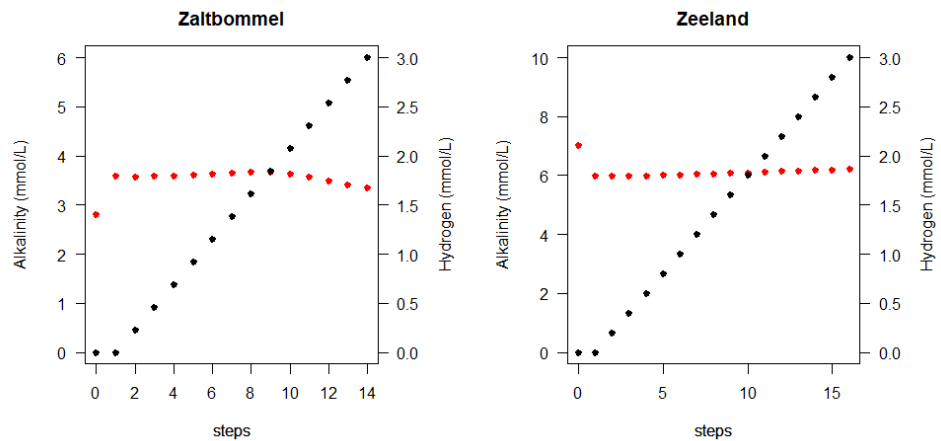

Figure 16: The equilibrium between alkalinity (left axis, red) and hydrogen (right axis, black) for each step of hydrogen addition in the model

The dissolved methane in the model of Zeeland remains around zero during each new equilibrium, while the dissolved methane in the model of Zaltbommel increases with each new equilibrium calculated (Figure 17).
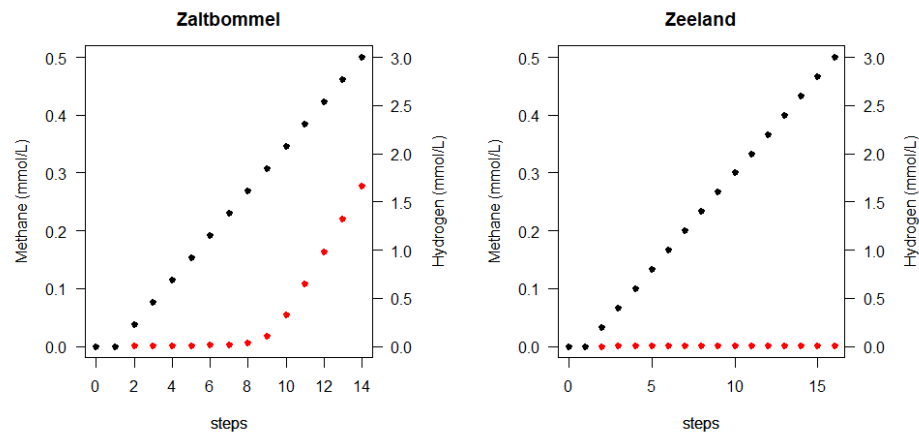
Figure 17:   The equilibrium between methane (left axis, red) and hydrogen (right axis, black) for each step of hydrogen addition in the model

The pH increases in the model of Zaltbommel during the first calculated equilibrium, while the pH decreases in the model of Zeeland during the first calculated equilibrium (Figure 18). After the first step, the pH stays relatively constant in both models.
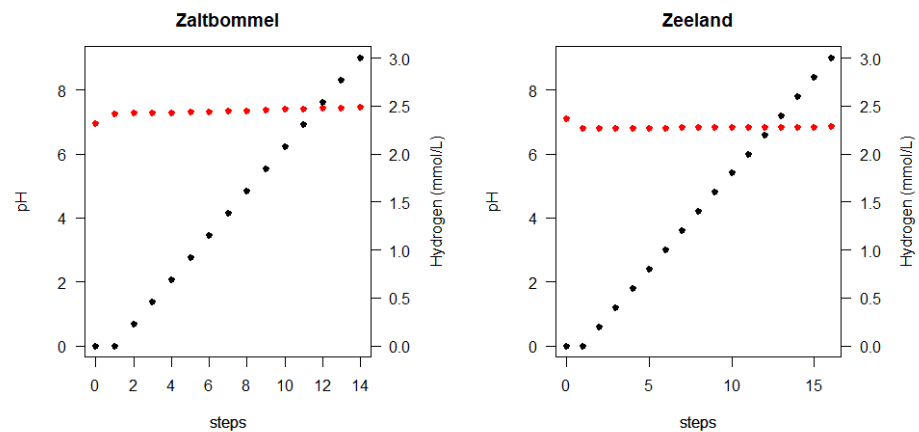
Figure 18:   The equilibrium between pH (left axis, red) and hydrogen (right axis, black) for each step of hydrogen addition in the model

Remainder parameters that have an output from the model and within the scope of the project are calcium and phosphorus. Calcium for the model of Zaltbommel increases in the first equilibrium calculated, then it decreases for each other equilibrium calculated (Appendix D: Figure 28, left). Calcium in the model of Zeeland slightly decreases with each new equilibrium calculated (Appendix D: Figure 28, right). Phosphorus remains constant in both models, during each new equilibrium calculated (Appendix D: Figure 29).

4.2.2   *Saturation indexes*

The model also calculates saturation indexes (SI) for mineral phases and gas phases. The phases considered are $CO_2(g)$, $H_2(g)$, $CH_4(g)$, goethite, siderite, pyrite,

hematite, Fe(OH)$_3$ (a), magnetite, and calcite. When the SI is below zero it implies that the water is undersaturated with the mineral. This will imply the dissolution of the mineral if it is present. When the SI is larger than zero the water is supersaturated with the mineral. This will imply precipitation of the mineral, which may be kinetically hindered. When the SI is zero, the water and the mineral are at chemical equilibrium.

For gasses when the SI is lower than zero, it means that the partial pressure is lower than one atmosphere. When the partial pressure is higher than zero, it means that the partial pressure is higher than one atmosphere.

In most cases, the SI has become closer to zero at the end of the run of the model for the mineral phases (Zaltbommel: goethite, siderite, hematite, magnetite, and calcite. Zeeland: goethite, hematite, magnetite, and calcite.) (Table 7). However, for calcite, it was assumed that the SI would be zero. In the Zaltbommel model, SI from pyrite goes from negative to positive, while the SI from Fe(OH)$_{3(a)}$ goes from positive to negative. In the Zeeland model, the SI from siderite becomes more positive and the SI from pyrite goes from negative to positive, while the SI from Fe(OH)$_{3(a)}$ goes from positive to negative.

For the gasses, the SI becomes closer to zero for CO$_2$ in the model of Zeeland, and H$_2$ and CH$_4$ in both models. The SI for CO$_2$ in the model of Zaltbommel becomes more negative.

Table 7: Initial and final saturation indexes of the model for both Zaltbommel and Zeeland

Species	SI initial (Zaltbommel)	SI final (Zaltbommel)	SI initial (Zeeland)	SI final (Zeeland)
CO$_2$ (g)	-1.79	-2.29	-1.67	-1.54
H$_2$ (g)	-21.92	-6.43	-63.53	-3.00
CH$_4$ (g)	-62.51	-3.50	NA	-3.37
Goethite	8.40	0.73	8.08	0.39
Siderite	0.77	0.50	0.44	0.5
Pyrite	-90.45	12.44	-92.67	13.51
Hematite	18.78	3.42	18.13	2.75
Fe(OH)$_3$ (a)	2.77	-4.79	2.44	-5.13
Magnetite	20.58	5.32	19.48	3.90
Calcite	-0.45	0	0.42	0

4.2.3   *Comparison between Fe(II), H$_2$S, and CH$_4$*

To compare the redox processes in the model, Fe(II), H$_2$S, and CH$_4$ are plotted together. In the model of Zaltbommel, the CH$_4$ starts to increase, when H$_2$S remains constant for each new calculated equilibrium after the 10th step (Figure 19). There is no link between Fe(II) and CH$_4$/H$_2$S in the model of Zaltbommel (Figure 19).

Figure 19:   The equilibrium between Fe(II) (left axis, red), H$_2$S (left axis, blue), CH$_4$ (left axis, green), and hydrogen (right axis, black) for each step of hydrogen addition in the model

After the second equilibrium, the increase in Fe(II) is slowing down while the H$_2$S starts to increase (Figure 20). For each other equilibrium, there is also no link between Fe(II) and H$_2$S/CH$_4$ (Figure 20). Also, the amount of CH$_4$ remains zero during each equilibrium (Figure 20).
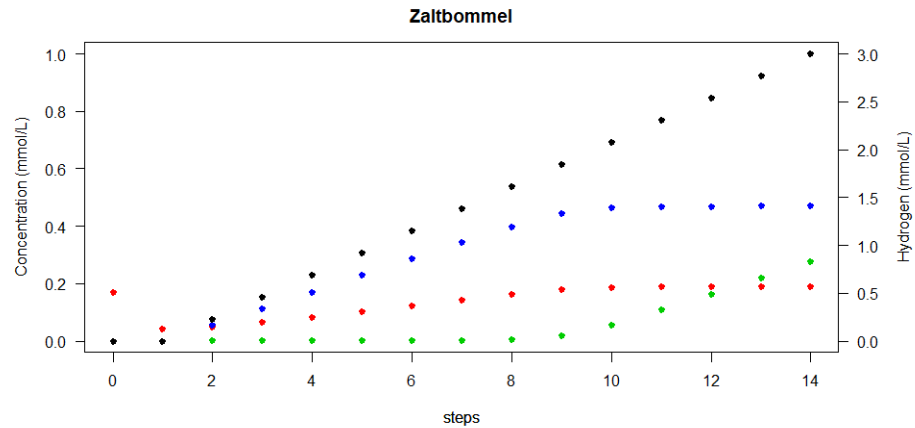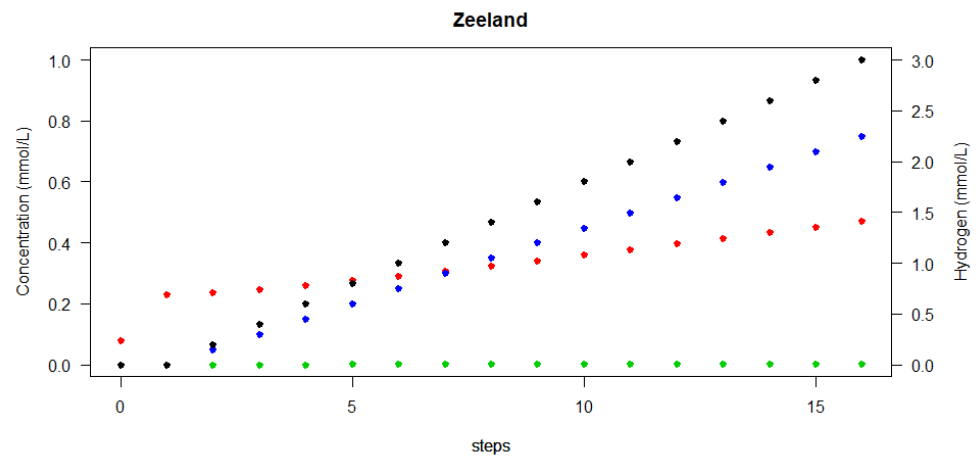

Figure 20:   The equilibrium between Fe(II) (left axis, red), H$_2$S (left axis, blue), CH$_4$ (left axis, red), and hydrogen (right axis, black) for each step of hydrogen addition in the model

5 Discussion

5.1 Assessment of methodology

The influence of leakage of subsurface stored hydrogen onto the groundwater chemistry is not well known as it has not been much researched experimentally. Studying the impact of leakage of hydrogen, therefore, consists of developing a method for experimental research. Designing a method from scratch involves detecting deficiencies of the method during the experiment. The deficiencies of the used method are discussed in this section and solutions are proposed to abolish these deficiencies.

5.1.1 *Loss of pressure in the keykeg® → consequences for hydrogen addition*

It was assumed that the keykeg® was suitable enough for retaining pressure on the groundwater during storage. However, the downside of the keykeg® is that the pressure is not maintained between the inner and outer wall while the filling head is coupled to the keykeg®.

When the filling head is not attached to the keykeg®, the pressure between the aluminum bag and the outer plastic wall is maintained. When the filling head is connected, it pushes, on the location of the red arrow, one layer of the plastic outer wall down (Figure 21). This opens two small holes, on the location of the red dot (Figure 21). Pressurized air between the inner and outer wall can escape from these two small holes.

The system is closed during the experiment by sealing these two small holes, but sealing takes a lot of effort and the reliability is not tested. This downside of the keykeg® is caused by the tubing for the hydrogen addition. The tube for the hydrogen addition goes through the filling head into the keykeg® and needs to be already in there during the filling of the keykeg®. The consequence is that the filling head cannot be removed after filling the keykeg® with groundwater, because the tube would then be removed. By plugging the filling head onto the keykeg®, these small holes in the upper part of the keykeg® are opened. This causes a pressure loss during the storage of the pumped-up groundwater. Maintaining the pressure is needed during storage because the gasses present in the pumped-up groundwater needs to be kept dissolved. To overcome the pressure loss in the keykeg® during storage, the best solution is to remove the tube for the hydrogen addition. When removed, the filling head does not need to be plugged on during storage and the pressure can be maintained on the pumped-up groundwater.
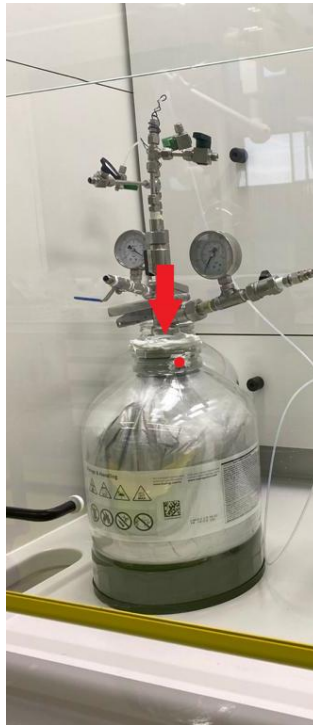
Figure 21:   The red arrow indicates where the filling head is attached, while the red dot indicates the location of one of the two holes. The other hole is on the other side of the keykeg®.

The loss of pressure is not a direct problem for the addition of hydrogen, as the hydrogen is added in the inner bag of the keykeg®. With the addition of hydrogen pressure is build up in the inner bag and this build-up pressure is maintained.

Future experiments can be conducted with the same method for the addition of the hydrogen, as the keykeg® is pressurized in the inner bag by the addition of the hydrogen gas. There is no gas leakage found in the filling head itself. However, there are other solutions to overcome the pressure loss during storage and retain dissolved gasses in the groundwater. One of the solutions is removing the extra tube which is connected only for the hydrogen addition. This implies that the addition of hydrogen gas should be added through the same input as the groundwater. The downside of this solution is that hydrogen is not bubbled through the groundwater, but just added as a layer on top of the groundwater. This increases the time for hydrogen dissolution into the groundwater. Another solution is by adding the hydrogen directly into the pressure vessels and not first into the keykeg®. However, the addition of hydrogen will then be less consistent.

5.1.2   Accuracy of the manometers

The manometers which were used during the experiment were simple manometers that belonged to the filling heads delivered by the keykegs®. However, these manometers have an offset when comparing their pressure with a calibrated manometer (Table 8). The consequence is an incorrect indication of the pressure between the inner- and outer walls. To work with these manometers, the offset in pressure should be taken into account during the entire experiment.

Table 8:   Offset of the manometers used in the experiment

Manometer used in the experiment	The offset of the calibrated manometer (bar)
Manometer 1	+ 0.4
Manometer 2	- 0.05
Manometer 3	+ 0.1
Manometer 4	- 0.03

Another problem with the manometers is the measuring precision by the manometer of the pressure between the inner and outer wall of the keykeg®. It is assumed that the pressure in the inner bag of the keykeg® is the same as the pressure between the inner and outer walls. However, the pressure indicated on the manometer on the keykeg® stayed around 1 bar during the addition of hydrogen in the keykeg® with the groundwater from Zaltbommel, while the pressure on the pressure relief valve indicated 3.5 bar. The manometer that was connected with the inner bag of the keykeg® also indicated 3.5 bar. To improve the method and the accuracy of the addition of hydrogen it is better to connect also a manometer directly to the inner bag of the keykeg®.

5.1.3   Use of plastic vessels

An important point of discussion is the use of plastic vessels (keykeg® and pressure vessels) in the experiment. Plastic materials are not gas-tight as gasses can diffuse through the walls of tubing and containers made of plastic (Kjeldsen, 1993). In the research of Kjeldsen (1993), he found that diffusion of oxygen through plastic material into anoxic water can be a serious problem for a series of plastic materials. The diffusion time can vary over orders of magnitude, depending upon both the gases and plastic materials (Kjeldsen, 1993). The diffusion of oxygen into anoxic water seems often to be a problem for plastic materials such as polyethylene, polypropylene, and Teflon (Kjeldsen, 1993). The research of Kjeldsen (1993) showed that the exchange of CO_2 and H_2 out of a plastic vessel is much slower than O_2 diffusing into the vessel. To anticipate this problem of oxygen diffusing into the Teflon pressure vessels, the incubations were stored in an argon purged glovebox during their incubation period. However, this could not prevent hydrogen loss by diffusion through the Teflon pressure vessel.

5.1.4   Comparison with other experimental studies

There is only one study where the effects of millimolar hydrogen concentrations on the groundwater in shallow aquifers were experimentally studied (Berta et al., 2018). The experimental setup of Berta et al. (2018) consisted of a high-pressure column experiment, instead of small pressure vessels that were used in this experiment. Advantages of using a high-pressure column experiment are the possibility to better control and maintain the pressure during the experiment and that it is a closed gas-tight system. In our approach, better control on a constant pressure between the loose elements in the set-up can be obtained by the use of correctly calibrated manometers every step. This will also give more insight into how well the method is protected against leakages in the system.

The disadvantage of a high-pressure column experiment is that it is less easy to set up experiments with different types of groundwater and sediments. Our approach enables us to study more types of groundwater and sediment at the same time in a relatively easy, inexpensive way. A high-pressure column experiment takes a lot of

effort to set up and is more expensive to build. Small incubation vessels are easier for incubation experiments at a smaller scale.

5.2 Effect of hydrogen on biogeochemical processes in the shallow aquifer

The main outcomes, related to biogeochemical processes, of the experimental results, are the consumption of hydrogen, an increase in pH, precipitation of dissolved iron, and consumption of methane during the experiments. However, most of the changes in the parameters during the experiment happen in both the reference incubations and the incubations with the added hydrogen. When interpreting the results focus should be given to whether the differences in concentration belong to the addition of hydrogen or belongs to the equilibration between the groundwater and the sediment or experimental artifacts.

5.2.1 Consumption of hydrogen

Hydrogen was removed from the system during the incubation experiments. Hydrogen was either oxidized during the incubation period or leaked through the incubation vessel. Leakage could have been possible through the wall of the Teflon vessel (Kjeldsen, 1993). However, it is assumed that the reactions between hydrogen and the biotic processes are faster than the leakage through the Teflon vessel. Kjeldsen (1993) experimentally showed that in a cylindrical reactor with a diameter of 10 cm, a volume of 1 liter, and a wall thickness of 2 mm, a hydrogen loss in the container of 5% was reached in 54 days. The vessels used in this experiment are about the same size (750 ml, ~10 cm diameter, heavy wall construction) as the containers in Kjeldsen (1993), indicating that leakage is not likely. The vessels were tested before the incubation experiment whether they would leak when pressurized. When tightened enough the vessels showed no indication of leakage when stored. Therefore, it is assumed that all hydrogen added was oxidized during the experiments. Oxidation of hydrogen also happens during the experimental study of Berta et al. (2018). Within the residence time in their experiment (6.3 hours), the dissolved concentration of hydrogen belonging to partial pressures below 3 bar was also oxidized before the solution reached the outlet (Berta et al., 2018). Now 2.34 mmol/L hydrogen was added into the system (corresponding to a partial pressure of 3 bar). A total of 1.17 mmol was thus available as a reductant in the redox processes as 500 ml groundwater was used during the experiment. As this is much larger than nanomolar concentrations in the sediment, the additional hydrogen makes hydrogen no longer limiting for hydrogenotrophic redox reactions and could have been used under the consumption of terminal electron acceptors.

5.2.2 Effects on redox processes

The redox processes likely happening are related to the consumption of Fe(III), SO_4^{2-} and HCO_3^- during the hydrogenotrophic reactions (Eq. 1-3). There are 1.17 millimoles of hydrogen available during the start of the experiment, which was all oxidized after 2 days in the groundwater from Zeeland and 7 days in the groundwater from Zaltbommel. Thermodynamically, it is expected that first iron reduction will take place, followed by sulphate reduction and methanogenesis (Lovley and Goodwin, 1986). However, with an excess hydrogen concentration, it might also be possible that the redox reactions will proceed parallel due to kinetics. To get an understanding of the dominant redox reaction in the experiment, the occurrence of these redox reactions should first be known.

With iron reduction, Fe(III) will be reduced towards Fe(II). There are respectively 0.09 millimoles and 0.042 millimoles of dissolved Fe initial in the groundwater of Zaltbommel and Zeeland available in the vessel, which in the groundwater from Zaltbommel and the 10-11m decreases towards 0.022 millimoles and for the other experiments towards zero. This implies that the dissolved fraction of iron precipitates during the experiments. The dissolved fraction of iron consists most likely mainly of Fe(II), because of the neutral pH of the experiment. Fe(III) forms minerals that at neutral pH are barely soluble (Straub et al., 2000). The decrease in concentration does therefore not indicate Fe(III) reduction. With Fe(III) reduction it is expected that there will be an increase in the dissolved iron fraction or the Fe(II) bearing minerals and a decrease in the Fe(III) bearing minerals (iron-oxides). Only in the incubation Zaltbommel (10-11m sediment), there is an increase of total Fe(II) in both the sediment and the groundwater (Table 9). In the other incubations, there is a decrease in Fe(II) (Table 9), indicating that Fe(III) reduction most likely did not take place. The increase of Fe(II) due to Fe(III) reducing should be 2.34 mmol, as there was 1.17 mmol of hydrogen available as reductant. There is only an increase of 0.36 mmol in incubation Zaltbommel (24-25m), so iron(III) reducing processes would have played a minor role. In the study of Berta et al. (2018), there is minor importance of Fe(III) reducing processes during the experiment. In their experiment, the dissolved Fe_{tot} concentrations stayed below the detection limit. However, it is difficult to compare Fe(III) reducing processes. Solely measuring dissolved Fe(tot) concentrations serves only as an indicator for identifying Fe(III) reduction processes, because precipitating mineral phases (i.e. FeS, $FeCO_3$) may limit the solubility of Fe(II) (Berta et al., 2018).

Table 9:   Absolute concentration of initial and final Fe(II) in the vessels with added hydrogen

	Initial Fe(II) (mmol)	**Final Fe(II) (mmol)**
Zaltbommel (24-25m)	0.63	0.33
Zaltbommel (10-11m)	0.95	1.31
Zeeland (24-25m)	0.59	0.17
Zeeland (10-11m)	0.90	0.34

The consumption of the dissolved fraction of iron (Fe(II)) in the other incubations could be explained by mineral precipitation. Minerals containing Fe(II) are Fe-carbonates, Fe-sulphides, and vivianite (Fe-phosphate) (Straub et al., 2000). These minerals are only formed in anoxic habitats under weakly acidic to neutral conditions (Straub et al., 2000). The trend of the iron-bearing minerals during the experiment could explain the consumption of the dissolved fraction of iron.

In the incubation of Zaltbommel (10-11m), there is a production of Fe-carbonates (Figure 12, upper left), Fe-sulphides (Figure 14, upper left), and consumption of phosphate (Appendix C: Figure 30, upper left). In the incubation of Zaltbommel (24-25m+Fe-oxide), there is a slight production of Fe-sulphides (Figure 14, upper right) and consumption of phosphate (Appendix C: Figure 30, upper right). In the incubation of Zeeland (10-11m sediment), there is only consumption of phosphate (Appendix C: Figure 20, bottom left) and no production of Fe(II) related mineral phases. In the incubation of Zeeland (24-25m+Fe-oxide sediment), there is a slight production (Figure 14, bottom right) and consumption of phosphate (Appendix C: Figure 30, bottom right). The dissolved iron fraction is most likely consumed by

mineral precipitation processes. The consumption of phosphate might be caused by the production of Fe(II)-phosphate minerals.

Unfortunately, there are no analyses of the concentration of SO_4^{2-} during the experiment, due to broken equipment. Due to the absence of these results, it cannot be directly assessed whether sulphate reduction took place during the experiment.

To investigate more directly the changes in concentration of SO_4^{2-} and the occurrence of sulphate reduction can be estimated based on the charge balances if the concentrations of all other major cations and anions are known. An aqueous solution is always electrical neutral, implying that the sum (in milliequivalents/liter) of the anions and the cations should always balance (Hill Laboratories, 2021). Hence, the difference between the sum of cations and that of anions equals the concentrations of SO_4^{2-} and Cl^- in milliequivalents/liter. Here, the cations considered are K^+, Mg^{2+}, Fe^{2+}/Fe^{3+}, H^+, and Ca^{2+}. The anions considered are HCO_3^-, CO_3^{2-}, Cl^- and SO_4^{2-}. To see the concentration differences in SO_4^{2-} the assumption is made that Cl^- is constant throughout the experiment, as the concentration from Cl^- is also analyzed on the IC.

There is a decline in the concentration of SO_4^{2-}/Cl^- during the incubation period (Figure 23). The decline is most apparent in the incubation Zaltbommel (24-25m). In the other incubations, the decline is minor. In Zeeland, the concentration of Cl^- is quite high as it is brackish groundwater. This makes it difficult to observe a difference in SO^{2-} taking into consideration analytical precision.
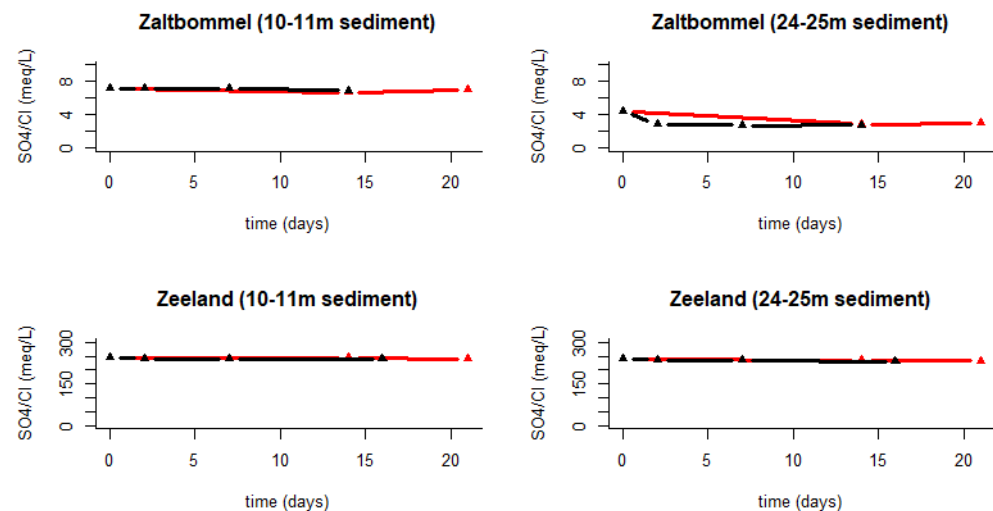
Figure 22:   Summed concentration of SO_4^{2-} and Cl^- against the time in days.

With the assumption that the concentration of Cl^- is constant throughout the experiment, the decline in concentration comes from a decline in SO_4^{2-}. In the experiment, there is 4.68 meq/L of hydrogen available. The consumption for all hydrogen can therefore be explained by sulphate reduction in the incubations with the groundwater from Zeeland (Table 10). For the incubations with the groundwater from Zaltbommel, only part of the hydrogen consumption can be explained by

sulphate reduction (Table 10). However, the concentrations of SO_4^{2-} also decrease in the reference incubations.

Table 10:   Decrease in sulphate concentrations (meq/L) based on the cation-anion balance

Incubation	SO_4^{2-} consumed (meq/L)
Zaltbommel (24-25m)	1.70
Zaltbommel (10-11m)	0.3
Zeeland (24-25m)	8.26
Zeeland (10-11m)	4.92

For methanogenesis HCO_3^- or CO_2 can be used as oxidants. However, there is no production of methane during the experiment, indicating methanogenesis does not occur. Furthermore, the concentration of HCO_3^- (as measured as alkalinity) increases during the experiments, thus reduction of bicarbonate is not likely. The concentration of CO_2 decreased during the experiment. There is also no methane production detected during the experiments by Berta et al. (2018). According to Berta et al. (2018), an increasing pH value might have inhibited methane formation because pH levels above 7-9 can prevent methanogenic activity. Here, the pH does not increase above 8. It might be possible that methanogenesis is not visible due to the time sequence of the experiment. According to Hansen et al. (2001), the methane formation rate in a shallow sandy aquifer ranges from 0.1 to 0.4 mM/yr. When applying this rate in our experiment, the methane production would be in the order of 0.3 - 1 μM/day under normal conditions. This rate of methane formation should have been visible in the experimental data. The absence of methanogenic activity can also be due to the lack of specialized microbes. Furthermore, methanogens are obligate anaerobes that metabolize only in anoxic conditions at redox levels with an Eh lower than 200 mV (Whiticar, 1999). Here, the Eh levels are not measured during the experiment. Furthermore, methanogens do not tolerate significant nitrate or nitrite levels, primarily due to the instability of their F_{420}-hydrogenase enzyme complex (Schonheit et al., 1981). As there are no results of the IC yet, this cannot be excluded from happening.

However, there is a pH increase in the incubations. The pH increase is observed in both the reference incubations and the incubations with hydrogen but rises slightly more in the hydrogen incubations. An increase in pH can be correlated with the consumption of H^+. H^+ is consumed during sulphate reduction and methanogenesis (Eq. 2-3). The increase in pH may therefore indicate a slight enhancement of sulphate reduction.

The increase in pH can also affect other species in the groundwater. An increasing pH can lead to the precipitation of calcium carbonate (Berta et al., 2018) and thus a decrease in calcium concentrations. Here, the concentration of calcium is relatively steady during the incubation period (Appendix C: Figure 29). So it is not likely that calcium precipitation took place.

The maximum amount of bacterial converted H_2 towards Fe(II), CH_4, and H_2S by the redox processes depends on the amount of available (and reactive) electron acceptors, Fe(III), carbon dioxide, and sulphate, and depends on the concentration of hydrogen in the groundwater (Hemme and Berk, 2018). The absence of methanogenesis can come from the fact that all H_2 is used during the reduction of

Fe(III) or SO_4^{2-}. However, in the four different incubations, there is no indication for Fe(III) reducing processes. The occurrence of sulphate reducing processes is likely when looking at the cation-anion balance. The removal of dissolved hydrogen could be either by adsorption or oxidation. With the oxidation of hydrogen, it should be able to detect the corresponding stimulation of Fe(III)/SO_4^{2-} reduction or methanogenesis, either due to the consumption of oxidant or production of reductant. The results do not indicate whether one of these processes delivers the dominating terminal electron acceptor.

The removal of hydrogen in the system can also be due to other processes. It might have been that hydrogen leaked out of the incubation vessel, but this is not very likely due to the different rates of hydrogen consumption depending on the sediment and groundwater.

Lost H_2 that is not converted by reducing processes, can go into mineral phases (Hemme and Berk, 2018). Hydrogen gas can also react with the clay fraction of the sediment. Didier et al. (2012) showed a 0.11 wt% hydrogen adsorption onto clays at 90°C under 0.45 bar. Didier et al. (2012) concluded that more than 18 m^3 of H_2 (g) per m^3 of clay rock could be adsorbed. In this experiment, the sediments which are used are sandy sediments, which makes adsorption onto clay of minor relevance.

In chapter 1 and chapter 2, it is already mentioned that abiotic processes related to hydrogen are not significant in environments with low temperatures and low pressures. Abiotic processes are most likely not occurring during the experiment, due to the low pressure and temperature. Besides, abiotic and biotic processes cannot be distinguished, as there are no sterilized incubations.

5.2.3   *Iron sequential extraction compared with the SI indexes from the model*
The production and consumption of several iron mineral phases during the experiment can be linked with dissolution and/or precipitation processes. The dissolution/precipitation of a mineral depends on the saturation index.
Easily soluble iron oxides ($Fe(OH)_3$) (targeted with the second step of the sequential extraction) dissolve during the experiment (Figure 12). Dissolution of amorphous iron oxides is also expected by the results from the model, where $Fe(OH)_3$ (a) has a negative saturation index (Table 8). One of the iron carbonates is siderite, which has a positive saturation index of 0.50 imposed in the model. Only one combination of the incubations shows a positive saturation index (e.g. production of Fe-carbonates) (Zaltbommel +10-11m sediment) during the experiment. The other incubations show contradicting results compared with the model. This might have to do with fixing the saturation index at 0.50 in the model.

5.3   Modelling results

The system is modelled based on the equilibrium between the sediments, groundwater, and the gas phase. With each step, a fraction of the hydrogen is added into the system causing a shift towards a new equilibrium. In reality, the biogenic redox system related to hydrogen is based on kinetics (Lassin et al., 2011) and a kinetic model will therefore better represent hydrogen-induced processes in the groundwater. Equilibrium batch modelling is also performed in other research (e.g. Hassannayeb et al., 2019).

5.3.1 Differences between the model of Zeeland and Zaltbommel

The model of the groundwater from Zaltbommel shows a more reduced redox condition than the model from Zeeland. The difference between the model resembling the groundwater from Zaltbommel and the model resembling the groundwater from Zeeland lies in the input concentrations of the aqueous phase. These differences in the initial concentrations might have an influence on the redox conditions during the equilibrium modelling.

The most likely reason is that the higher sulphate concentration influences the pe value. The redox potential (pe) value drops less when equilibrating with an addition of hydrogen (towards -3.2) than the redox potential (pe) from the model which resembles the groundwater from Zaltbommel (towards -4.3) (Figure 22).
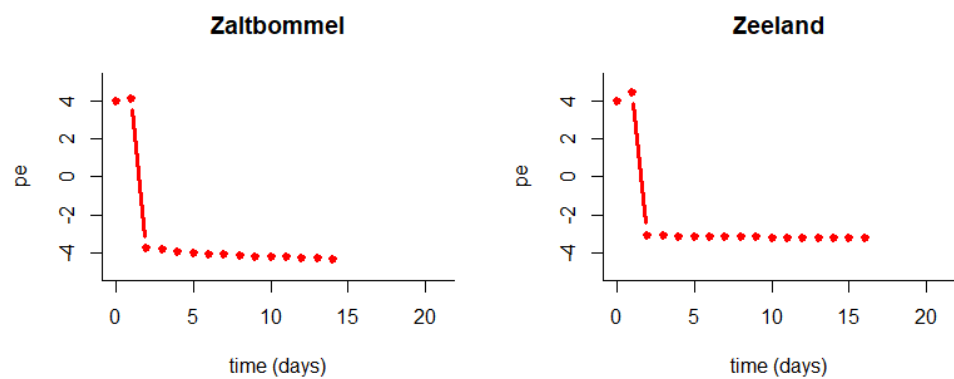

Figure 23:   Pe plotted against the time for the model resembling the groundwater from
Zaltbommel and the model resembling the groundwater from Zeeland

The differences in sulphate concentrations come most likely from the difference in fresh and brackish groundwater. Any input of hydrogen into (highly) saline fluid-bearing systems will most probably force a decrease in pH conditions (Pudlo et al., 2013). By introducing more millimoles of hydrogen in the model the redox potential of the system decreased and the pH of the system increased.

Besides, the model of Zaltbommel shows a better correlation with the experimental results. The model of Zaltbommel reaches the same equilibrium value for pH and alkalinity (Table 11). However, the model shows the production of methane and iron(II), while this is not the case in the experiments. The increase in methane concentrations in the model might be due to equilibration between the redox couple CH_4-HCO_3^-. The absence of methane in the experimental results might indicate that equilibrium has not been reached in the experiments.

Table 11: Equilibrium values of the pH and the alkalinity for the model and the incubation experiments

Zaltbommel			
Parameter	Model	10-11m sediment	24-25m sediment
pH	7.46	7.53	7.79
Alkalinity (mmol/L)	3.34	3.87	4.17
Zeeland			
Parameter	Model	10-11m sediment	24-25m sediment
pH	6.85	7.63	7.88
Alkalinity (mmol/L)	6.22	9.77	10.48

There is no clear correlation between the equilibrium values of the model of Zeeland and the experimental results. The pH and alkalinity values are lower in the model (Table 11). This might be caused by the simulation of redox processes in the model, which were not the same as in the experiment.

5.3.2   *Redox processes occurring in the model*
The model shows that the main disturbances are the pH increase/decrease, the decrease in the redox potential, and the production of H_2S and CH_4. The pH increase and the decrease in the redox potential result from the hydrogen introduced in the system (Lassin et al., 2011). This disturbance modifies the aqueous speciation and the minerals-solution equilibrium conditions (Lassin et al., 2011). Disturbances in the aqueous speciation are induced by the redox processes

After the addition of 0.23 millimoles of hydrogen in the model of Zaltbommel, the concentration of Fe(III) has decreased to zero and the concentration of Fe(II) increased. This indicates that the available concentration of Fe(III) is used in Fe(III) reduction in the first step of hydrogen addition. For the model of Zeeland, the redox equilibrium between Fe(II) and Fe(III) does not indicate Fe(III) reduction after the addition of hydrogen.

The increase in Fe(II) in the model comes from the dissolution of mineral phases. The only Fe-mineral phase present in the model is siderite. The concentration of siderite decreases during the run of the model with 0.14 mmol/L for the groundwater from Zaltbommel and 0.24 mmol/L for the groundwater from Zeeland. The Fe(II) concentration increases with 0.15 mmol/L for the groundwater from Zaltbommel and with 0.24 mmol/L for the groundwater from Zeeland.

The redox equilibrium between SO_4^{2-} and H_2S is affected by the addition of hydrogen. With each addition of 0.2 millimoles of hydrogen in the model of Zeeland and 0.23 millimoles in the model of Zaltbommel, the amount of SO_4^{2-} decreases while the amount of H_2S increases in a new calculated equilibrium. This is caused by the occurrence of sulphate reduction in the groundwater. After the addition of 2.3 millimoles of hydrogen in the model of Zaltbommel, all SO_4^{2-} is depleted. The SO_4^{2-} does not get depleted in the model of Zeeland, as 3 millimoles of hydrogen are not sufficient to oxidize all SO_4^{2-}.

To explore the occurrence of Fe(III) reduction, sulphate reduction, and methanogenesis in the model, the equilibrium values of Fe(II), H_2S and CH_4 are compared after each addition of hydrogen.

For Zaltbommel, there is no indication of Fe(III) reducing processes. After the initial addition hydrogen sulphate reduction takes place until 2.3 millimoles of hydrogen are added. At that point, the sulphate concentration is depleted and methanogenesis takes over, until the last equilibrium with 3 millimoles of hydrogen. For Zeeland, sulphate reduction takes place after hydrogen addition. This takes place after each new addition of hydrogen, as the sulphate in the groundwater does not get depleted and sulphate reduction is thermodynamically favourable.

Hassannayebi et al. (2019) state that the findings from their equilibrium batch model indicate that potential redox couples can play a big role in the consumption of hydrogen. Here, in both models, the main redox couples are $H_2S-SO_4^2$ and CH_4-HCO_3^-. The redox couple Fe(III)/Fe(II) does not play a role in the hydrogen dynamics for the model of Zaltbommel and only a minor role in the model of Zeeland, due to the absence of Fe(III) oxides. The equilibrium batch model constructed by Hassannayebi et al. (2019) also identifies CH_4-HCO_3^- and $H_2S-$$SO_4^{2-}$ as the main redox couples contributing to the consumption of hydrogen.

5.4 Implications and further research

5.4.1 Implications

The implications of leakage of hydrogen onto the geochemical composition of shallow aquifers show differences between the model and the experimental results. According to the experimental results, it is not likely that there will be Fe(III) reduction or methanogenesis. There might be sulphate reduction taking place according to the cation-anion balance, which results in the production of hydrogen sulphide. Hydrogen sulfide gas is toxic by inhalation and therefore the production of hydrogen sulfide in large quantities is a threat to the environment near the leakage.

The model results show other implications for the environment, which are not verified in the experimental results. The model clearly shows enhanced sulphate reduction due to the addition of hydrogen, and thus the production of hydrogen sulphide. However, when all sulphate is consumed, the model shows that methanogenesis takes over. This produces methane. Methane is not toxic to the environment, but it is a member of the greenhouse gasses. Besides, methane is quite flammable, and producing a large amount of methane near the borehole might increase the risks of failures. Furthermore, the model shows that the groundwater will become more alkaline in the case of low sulphate concentrations, and more acidic in the case of high sulphate concentrations.

5.4.2 Further research

Further research is necessary for understanding the exact influence of hydrogen on the biotic or abiotic processes in shallow aquifers. It needs to be better investigated whether the changes in the parameters can be ascribed to equilibrium processes between the sediment and the groundwater or to the addition of the hydrogen. An improvement would be to sample reference incubations and incubations with added hydrogen at the same time in the first few days. This will give a better insight into the influence of hydrogen on the redox reactions.

Furthermore, it is interesting to add hydrogen at certain intervals in the experimental set-up. Between these intervals, time can be given for the system to go back into equilibrium. With these intervals, insight can be gathered on how long it takes for the system to establish equilibrium and at which concentration of added hydrogen the system will no longer be influenced.

It is also interesting to explore the velocity of the established redox reactions. Berta et al. (2018) already showed that a partial pressure of hydrogen higher than 2 bar does not affect the velocity of the established redox reactions.

6   Conclusion

In this chapter, the research questions are assessed based on the experimental and simulated data.

Does leakage of H_2 into groundwater result in the consumption of Fe(III) oxyhydroxides, SO_4^{2-} and HCO_3^- with associated production of Fe(II), H_2S, and CH_4?

During the experiment, the hydrogen in the incubations does decrease. However, the consumption of hydrogen does not correlate with the outcomes of the experiment. Instead, there is not an increased consumption of Fe(III) oxyhydroxides in the incubations with added hydrogen and the dissolved Fe decreases. There is only in one incubation (Zaltbommel (10-11m sediment)) a production of Fe(II) in the Fe-carbonates phase. There is no consumption of HCO_3^- but a production associated with the pH shift. Furthermore, there is no production of CH_4 in the incubations. There seems to be a consumption of SO_4^{2-}, which can be explained by enhanced sulphate reduction. However, this consumption is based on the cation-anion balance due to a lack of results from the IC. The model did show consumption of SO_4^{2-}, production of H_2S, and production of CH_4, indicating sulphate reduction and methanogenesis.
Thus, experimental evidence for the stimulation of hydrogenotrophic redox reactions was not provided. Further laboratory research of these redox processes is required to improve modelling efforts.

What is the dominating TEA used to oxidize naturally present electron donors and will there be a shift in the dominating TEA by the presence of high H_2 concentrations in the groundwater?

The experimental results do not indicate biotic redox processes for both the reference incubations and the incubations with added hydrogen. Therefore the experimental evidence is not provided to conclude what the dominating TEA is and whether there will be a shift. The calculated cation-anion balance indicates a decrease of sulphate, implying sulphate reduction as dominating TEA.
From the modelling results, it becomes clear that under enhanced hydrogen conditions sulphate reduction is the main redox process, thus the dominating TEA is SO_4^{2-}. When all SO_4^{2-} is reduced in the sediment due to the addition of hydrogen methanogenesis takes over as the dominant process.
The dominating TEA also depends on the sediments and groundwater used during the experiment. To acquire knowledge about the dominating TEA in certain possible UHS locations site-specific laboratory experiments are needed.

What is the effect of leakage of H_2 on the iron mineral composition of the aquifer sediment?

There is only an effect on the iron mineral composition in the incubation of Zaltbommel (10-11 m). This incubation shows the production of Fe-carbonates. In the other incubation with the groundwater from Zaltbommel, the reference incubation and the incubation with added hydrogen show the same trend, indicating no effect of hydrogen. In the incubations with the groundwater from Zeeland, there

is first dissolution of Fe-carbonates, which happens in both the reference incubations and the incubations with hydrogen. In the incubations with hydrogen, there is a slight increase in the production of Fe-carbonates at the end of the incubation period, which might be caused by the addition of hydrogen.

The easily reducible iron oxides and iron sulphide show in all incubations the same trend in the reference incubations and the incubations with added hydrogen. This indicates that there is not likely any effect of the leakage of hydrogen.

Will the redox reactions initiated by an increased H_2 concentration of hydrogen cause a change in groundwater pH and does this influence other, non-redox hydrogeochemical processes?

There is an increase in pH in the experimental results. However, it cannot directly be ascribed due to the redox reactions initiated by an increased concentration of hydrogen, as the reference incubations also show an increase in pH. Besides, there is no clear indication for sulphate reduction or methanogenic activity raising the pH. The pH increase does not influence the dissolution or precipitation of calcium carbonate, as the concentration of calcium is steady throughout the experiment. As there is no consumption of calcium during the experiment, it implies that the SI of calcite is already above 0 initially.

7 References

Adhikari, R. R., Glombitza, C., Nickel, J. C., Anderson, C. H., Dunlea, A. G., Spivack, A. J. & Kallmeyer, J. (2016). Hydrogen utilization potential in subsurface sediments. *Frontiers in microbiology*, *7*, 8.

AIP Conference Proceedings 2033, 030001 (2018); https://doi.org/10.1063/1.5067017

Allan, M. M., Turner, A., & Yardley, B. W. (2011). Relation between the dissolution rates of single minerals and reservoir rocks in acidified pore waters. *Applied geochemistry*, *26*(8), 1289-1301.

Alpermann, T., & Ostertag-Henning, C. (2019, April). Abiotic Redox Reactions of H2 with Iron- containing Minerals under Geologic Storage Conditions. In *EAGE/DGMK Joint Workshop on Underground Storage of Hydrogen* (Vol. 2019, No. 1, pp. 1-3). European Association of Geoscientists & Engineers.

Bai, M., Song, K., Sun, Y., He, M., Li, Y., & Sun, J. (2014). An overview of hydrogen underground storage technology and prospects in China. *Journal of Petroleum Science and Engineering*, *124*, 132-136.

Berta, M., Dethlefsen, F., Ebert, M., Schäfer, D., & Dahmke, A. (2018). Geochemical effects of millimolar hydrogen concentrations in groundwater: an experimental study in the context of subsurface hydrogen storage. *Environmental science & technology*, *52*(8), 4937-4949.

Brandt, F., Bosbach, D., Krawczyk-Bärsch, E., Arnold, T., & Bernhard, G. (2003). Chlorite dissolution in the acid pH-range: a combined microscopic and macroscopic approach. *Geochimica et Cosmochimica Acta*, *67*(8), 1451-1461.

Carden, P. O., & Paterson, L. (1979). Physical, chemical and energy aspects of underground hydrogen storage. *International Journal of Hydrogen Energy*, *4*(6), 559-569.

Claff, S. R., Sullivan, L. A., Burton, E. D., & Bush, R. T. (2010). A sequential extraction procedure for acid sulfate soils: partitioning of iron. *Geoderma*, *155*(3-4), 224-230.

Conrad, R. (1999). Contribution of hydrogen to methane production and control of hydrogen concentrations in methanogenic soils and sediments. *FEMS microbiology Ecology*, *28*(3), 193-202.

Conte, M., Iacobazzi, A., Ronchetti, M., & Vellone, R. (2001). Hydrogen economy for a sustainable development: state-of-the-art and technological perspectives. *Journal of power sources*, *100*(1-2), 171-187.

Cord-Ruwisch, R., Seitz, H. J., & Conrad, R. (1988). The capacity of hydrogenotrophic anaerobic bacteria to compete for traces of hydrogen depends on the redox potential of the terminal electron acceptor. *Archives of Microbiology*, *149*(4), 350-357.

Davison, J. (2009). Electricity systems with near-zero emissions of CO2 based on wind energy and coal   gasification with CCS and hydrogen storage. *International Journal of Greenhouse Gas Control*, *3*(6), 683-692.

DBI GUT. (2017). *The effects of hydrogen injection in natural gas networks for the Dutch underground storages*. The effects of hydrogen injection in natural gas networks for the Dutch underground storages.pdf

Didier, M., Leone, L., Greneche, J. M., Giffaut, E., & Charlet, L. (2012). Adsorption of hydrogen gas   and redox processes in clays. *Environmental Science & Technology*, *46*(6), 3574-3579.

Energy in the Netherlands. (2018). EBN. https://www.ebn.nl/wp-content/uploads/2018/04/EBN-poster-numbers2016.pdf

Engineering ToolBox. (n.d.). Engineering Toolbox. Retrieved January 10, 2021, from https://www.engineeringtoolbox.com/

Feldmann, F., Hagemann, B., Ganzer, L., & Panfilov, M. (2016). Numerical simulation of hydrodynamic and gas mixing processes in underground hydrogen storages. *Environmental Earth Sciences*, *75*(16), 1165.

Fischer, S., Liebscher, A., Wandrey, M., & CO2SINK Group. (2010). CO2–brine–rock interaction—First results of long-term exposure experiments at in situ P–T conditions of the Ketzin CO2 reservoir. *Geochemistry*, *70*, 155-164.

Flaathen, T. K., Gislason, S. R., Oelkers, E. H., & Sveinbjörnsdóttir, Á. E. (2009). Chemical evolution of the Mt. Hekla, Iceland, groundwaters: A natural analogue for CO2 sequestration in basaltic rocks. *Applied Geochemistry*, *24*(3), 463-474.

Flesch, S., Pudlo, D., Albrecht, D., Jacob, A., & Enzmann, F. (2018). Hydrogen underground storage—Petrographic and petrophysical variations in reservoir sandstones from laboratory experiments under simulated reservoir conditions. *International Journal of Hydrogen Energy*, *43*(45), 20822-20835.

Gabrielli, P., Poluzzi, A., Kramer, G. J., Spiers, C., Mazzotti, M., & Gazzani, M. (2020). Seasonal energy storage for zero-emissions multi-energy systems via underground hydrogen storage. *Renewable and Sustainable Energy Reviews*, *121*, 109629.

Griffioen, J., Vermooten, S., & Janssen, G. (2013). Geochemical and palaeohydrological controls on the composition of shallow groundwater in the Netherlands. *Applied geochemistry*, *39*, 129-149.

Hagemann, B., Rasoulzadeh, M., Panfilov, M., Ganzer, L. and Reitenbach, V., 2015. Mathematical modeling of unstable transport in underground hydrogen storage. *Environmental Earth Sciences*, *73*(11), pp.6891-6898.

Hagemann, B., Rasoulzadeh, M., Panfilov, M., Ganzer, L., & Reitenbach, V. (2016). Hydrogenization of underground storage of natural gas. *Computational Geosciences*, *20*(3), 595-606.

Hagemann, B. (2018). *Numerical and analytical modeling of gas mixing and bio-reactive transport during underground hydrogen storage* (Vol. 50). Cuvillier Verlag.

Hansen, L. K., Jakobsen, R., & Postma, D. (2001). Methanogenesis in a shallow sandy aquifer, Rømø, Denmark. *Geochimica et Cosmochimica Acta*, *65*(17), 2925-2935.

Hassannayebi, N., Azizmohammadi, S., De Lucia, M., & Ott, H. (2019). Underground hydrogen storage: application of geochemical modelling in a case study in the Molasse Basin, Upper Austria. *Environmental Earth Sciences*, *78*(5), 177.

Hemme, C., & van Berk, W. (2017). Potential risk of H2S generation and release in salt cavern gas storage. *Journal of Natural Gas Science and Engineering*, *47*, 114-123.

Hemme, C., & Van Berk, W. (2018). Hydrogeochemical modeling to identify potential risks of underground hydrogen storage in depleted gas fields. *Applied Sciences*, *8*(11), 2282.

Henry, W. (1803). III. Experiments on the quantity of gases absorbed by water, at different temperatures, and under different pressures. *Philosophical Transactions of the Royal Society of London*, (93), 29-274.

Higbie, R. (1935). Penetration theory leads to use of the contact time in the calculation of the mass transfer coefficients in the two film theory. *Trans. Am. Inst. Chem. Engrs 31*, *365*.

Hill Laboratories. (2021). *Cation-Anion balances*. https://www.hilllaboratories.com/assets/Uploads/13213v6.pdf

Jakobsen, R., Albrechtsen, H. J., Rasmussen, M., Bay, H., Bjerg, P. L., & Christensen, T. H. (1998). H2 concentrations in a landfill leachate plume (Grindsted, Denmark): In situ energetics of terminal electron acceptor processes. *Environmental Science & Technology*, *32*(14), 2142-2148.

Jakobsen, R., & Postma, D. (1999). Redox zoning, rates of sulfate reduction and interactions with Fe-reduction and methanogenesis in a shallow sandy aquifer, Rømø, Denmark. *Geochimica et Cosmochimica Acta*, *63*(1), 137-151.

Jørgensen, B. B., Isaksen, M. F., & Jannasch, H. W. (1992). Bacterial sulfate reduction above 100 C in deep-sea hydrothermal vent sediments. *Science*, *258*(5089), 1756-1757.

Kjeldsen, P. (1993). Evaluation of gas diffusion through plastic materials used in experimental and sampling equipment. *Water research*, *27*(1), 121-131.

Lassin, A., Dymitrowska, M., & Azaroual, M. (2011). Hydrogen solubility in pore water of partially saturated argillites: Application to Callovo-Oxfordian clayrock in the context of a nuclear waste geological disposal. *Physics and Chemistry of the Earth, Parts A/B/C*, *36*(17-18), 1721-1728.

Lewis, W. K., & Whitman, W. G. (1924). Principles of gas absorption. *Industrial & Engineering Chemistry*, *16*(12), 1215-1220.

Lopez Ortiz, A., & Harrison, D. P. (2001). Hydrogen production using sorption-enhanced reaction. *Industrial & engineering chemistry research*, *40*(23), 5102-5109.

Lovley, D. R., & Goodwin, S. (1988). Hydrogen concentrations as an indicator of the predominant terminal electron-accepting reactions in aquatic sediments. *Geochim. Cosmochim. Acta*, *52*(12), 2993-3003.

Monod, J. (1949). The growth of bacterial cultures. *Annual review of microbiology*, *3*(1), 371-394.

Moser, A. (1985). Kinetics of batch fermentations. In: Rehm, H.J. and Reed, G. (Eds.) *Biotechnology (Vol.2)*, VCH Verlagsgesellschaft mbH, Federal Republic of Germany, 253.

Nernst, W. (1904). Theorie der Reaktionsgeschwindigkeit in heterogenen Systemen. *Zeitschrift für physikalische Chemie*, *47*(1), 52-55.

NIST Chemistry WebBook. (2018, October 16). NIST Webbook. https://webbook.nist.gov/chemistry/

Panfilov, M. (2010). Underground storage of hydrogen: in situ self-organisation and methane generation. *Transport in porous media*, *85*(3), 841-865.

Panfilov, M. (2016). Underground and pipeline hydrogen storage. In *Compendium of hydrogen energy* (pp. 91-115). Woodhead Publishing.

Parkhurst, D. L., & Appelo, C. A. J. (1999). User's guide to PHREEQC (Version 2): A computer program   for speciation, batch-reaction, one-dimensional transport, and inverse geochemical calculations. *Water-resources investigations report*, *99*(4259), 312.

Pfeiffer, W. T., Al Hagrey, S. A., Köhn, D., Rabbel, W., & Bauer, S. (2016). Porous media hydrogen storage at a synthetic, heterogeneous field site: numerical simulation of storage operation and geophysical monitoring. *Environmental Earth Sciences*, *75*(16), 1177.

Poulton, S. W., & Canfield, D. E. (2005). Development of a sequential extraction procedure for iron: implications for iron partitioning in continentally derived particulates. *Chemical geology*, *214*(3-4), 209-221.

Pudlo, D., Ganzer, L., Henkel, S., Kühn, M., Liebscher, A., De Lucia, M., & Gaupp, R. (2013). The H2STORE project: hydrogen underground storage–A feasible way in storing electrical power in geological media?. In *Clean Energy Systems in the Subsurface: Production, Storage Conversion* (pp. 395-412). Springer, Berlin, Heidelberg.

Rhino, K., Loisy, C., Cerepi, A., Garcia, B., Rouchon, V., El Khamlichi, A., & Noirez, S. (2018). Characterization and quantification of a CO2 and CH4 leakage experiment from a well into the carbonate vadose zone. *International Journal of Greenhouse Gas Control*, *77*, 55-69.

Shimko, M. A. (2008, March). High-Pressure Electrolysis Optimized for Supplying Premium Power. In *The NHA Annual Hydrogen Conference 2008*.

Straub, K. L., Benz, M., & Schink, B. (2001). Iron metabolism in anoxic environments at near neutral pH. *FEMS microbiology ecology*, *34*(3), 181-186.

Taylor, J. B., Alderson, J. E. A., Kalyanam, K. M., Lyle, A. B., & Phillips, L. A. (1986). Technical and economic assessment of methods for the storage of large quantities of hydrogen. *International Journal of Hydrogen Energy*, *11*(1), 5-22.

Thiel, J., Byrne, J. M., Kappler, A., Schink, B., & Pester, M. (2019). Pyrite formation from FeS and H2S is mediated through microbial redox activity. *Proceedings of the National Academy of Sciences*, *116*(14), 6897-6902.

Timmis, K. N. (ed.) (2010). Handbook of Hydrocarbon and Lipid Microbiology, DOI 10.1007/978-3-540-77587- 4_36,# Springer-Verlag Berlin Heidelber

TNO geologische dienst Nederland. (n.d.). Ondergrondgegevens. Dinoloket. Retrieved December 7, 2020, from https://www.dinoloket.nl/ondergrondgegevens

Toor, H. L., & Marchello, J. M. (1958). Film-penetration model for mass and heat transfer. *AIChE Journal*, *4*(1), 97-101.

Truche, L., Berger, G., Destrigneville, C., Pages, A., Guillaume, D., Giffaut, E., & Jacquot, E. (2009). Experimental reduction of aqueous sulphate by hydrogen under hydrothermal conditions: implication for the nuclear waste storage. *Geochimica et Cosmochimica Acta*, *73*(16), 4824- 4835.

Truche, L., Berger, G., Destrigneville, C., Guillaume, D., & Giffaut, E. (2010). Kinetics of pyrite to pyrrhotite reduction by hydrogen in calcite buffered solutions between 90 and 180 C: Implications for nuclear waste disposal. *Geochimica et Cosmochimica Acta*, *74*(10), 2894- 2914.

Truche, L., Jodin-Caumon, M. C., Lerouge, C., Berger, G., Mosser-Ruck, R., Giffaut, E., & Michau, N. (2013). Sulphide mineral reactions in clay-rich rock induced by high hydrogen pressure. Application to disturbed or natural settings up to 250 C and 30 bar. *Chemical Geology*, *351*, 217-228.

Van Loon, G. W., & Duffy, S. J. (2017). *Environmental chemistry: a global perspective*. Oxford university press.

Van Wageningen, H. S., Sötemann, S. W., Ristow, N. E., Wentzel, M. C., & Ekama, G. A. (2006). Development of a kinetic model for biological sulphate reduction with primary sewage sludge as substrate. *Water SA*, *32*(5).

Velde, B. B., & Meunier, A. (2008). *The origin of clay minerals in soils and weathered rocks*. Springer Science & Business Media.

Viollier, E., Inglett, P. W., Hunter, K., Roychoudhury, A. N., & Van Cappellen, P. (2000). The ferrozine method revisited: Fe (II)/Fe (III) determination in natural waters. *Applied geochemistry*, *15*(6), 785-790.

Watson, I. A., Oswald, S. E., Mayer, K. U., Wu, Y., & Banwart, S. A. (2003). Modeling kinetic processes controlling hydrogen and acetate concentrations in an aquifer-derived microcosm. *Environmental science & technology*, *37*(17), 3910-3919.

Whiticar, M. J. (1999). Carbon and hydrogen isotope systematics of bacterial formation and oxidation of methane. *Chemical Geology*, *161*(1-3), 291-314.

Yekta, A. E., Pichavant, M., & Audigane, P. (2018). Evaluation of geochemical reactivity of hydrogen in sandstone: Application to geological storage. *Applied Geochemistry*, *95*, 182-194.

8   Appendix

8.1   Appendix A: Film theory

In 1924, Lewis-Whitman further developed the film theory into a two film theory. The film theory assumes there are two stagnant film layers at the interface. Mass transfers across these films occurs by molecular diffusion and the bulks of gas and liquid are homogeneous with respect to the solute (Lewis-Whitman, 1924).

The film theory describes both the gas phase transport (Eq. 7) and the liquid phase transport (Eq. 8). When the system is in steady state it implies that $J = J_g = J_k$.

$$J_g = k_g(C_g - C_{g,i}) \tag{7}$$

Where
- J_g is the flux from the gas phase into the liquid phase [mol/(m²*s)]
- K_g is the mass transfer coefficient for the gas interface [m/s]
- C_g is the concentration of the gas in the bulkphase [mol/m³]
- $C_{g,i}$ is the concentration of the gas at the interface [mol/m³]

$$J_l = k_l(C_{li} - C_l) \tag{8}$$

Where
- J_l is the flux from the gas phase into the liquid phase [mol/(m²*s)]
- K_l is the mass transfer coefficient for the liquid interface [m/s]
- C_l is the concentration of the liquid in the bulkphase [mol/m³]
- $C_{l,i}$ is the concentration of the liquid at the interface [mol/m³]

With the film model and certain assumptions the time it takes to reach equilibrium can be calculated (e.g. after the addition of hydrogen gas into the keykeg®). First, the hydrogen concentration in the liquid phase and the gas phase under a pressure of three bar should be known. The concentration of hydrogen in the liquid phase is 2.34 mol/m3, calculated with Henry's law (Eq. 6). The concentration of hydrogen in the gas phase is 132.15 mol/m3, calculated with the gas law (Eq. 9).

$$\frac{n}{V} = \frac{P}{RT} \tag{9}$$

Where
- n is the amount of moles [mol]
- V is the volume [m³]
- P is the pressure [pascal]
- R is the universal gas constant [J/(mol*k)]
- T is the temperature [k]

The first assumption is equal concentrations in the bulk and at the gas-liquid surface. Implying that liquid and gas phase are homogeneous. In equation 10, m (equilibrium constant) can be calculated. The equilibrium constant is based on the ratio of the concentrations of gas and liquid at the interface when the system is in equilibrium. $C_{g,i}$ is the concentration at the gas interface and $C_{l,i}$ is the concentration at the liquid interface. The equilibrium constant can be determined at the given

conditions, resulting in a value of 0.0196. The value of the equilibrium constant is below one, which indicates hydrogen prefers to be in the gas phase than in the liquid phase (Highbie, 1935; Toor and Marchello, 1958). Furthermore, when m is low, mass transfer is controlled by the liquid film resistance (k_L) (Highbie, 1935; Toor and Marchello, 1958).

$$m = \frac{c_{l,i}}{c_{g,i}}$$

(10)

Where
- m is the equilibrium consant
- $C_{l,i}$ is the concentration of the liquid at the interface [mol/m^3]
- $C_{g,i}$ is the concentratin of the gas at the interface [mol/m^3]

By combining equations 7, 8 and 10, equation 11 is obtained. With this equation, the flux of hydrogen at the surface can be calculated.

$$J_{H_2} = \frac{C_g * \frac{C_l}{m}}{\frac{1}{k_g} + \frac{1}{m*k_l}}$$

(11)

Where
- J_{H2} is the flux of hydrogen gas into the liquid phase [mol/(m^2*s)]

Secondly, to calculate the mass transfer coefficient (k) for either the liquid or the gas phase, the diffusion coefficient (D) is divided by the stagnant film thickness (d) (Eq. 12). The diffusion coefficient of hydrogen is 4.58 x 10^{-5} cm^2/s at atmospheric pressure and 20 °C (Engineering toolbox). The diffusion coefficient is assumed to not change with an increase in pressure. For the stagnant film thickness in a hydrogen-water system, Beckers and Glatsmaier (AIP Conference Proceedings, 2018) use 10 to 100 mm for the liquid surface and 0.1 to 1 cm for gas surface. Here, the stagnant film thickness was assumed to be 100 mm.

$$k = \frac{D}{\delta_n}$$

(12)

Where
- K is the mass transfer coefficient [m/s]
- D is the diffusion coefficient [m^2/s]
- d is the film thickness [m]

Thirdly, the mass flow of hydrogen from liquid phase to the gas phase is assumed to be 0, due to the high gas phase resistance k_g. For less soluble gasses like H$_2$, such as N$_2$ and O$_2$ (m is low), mass transfer is controlled by liquid film resistance (Highbie, 1935; Toor and Marchello, 1958). Lastly, it is assumed there is initially no concentration of hydrogen in the liquid phase. This reduces equation 9 to equation 13, which describes the flux of hydrogen gas at the surface of the system. The flux of hydrogen into the groundwater is calculated to be 1.1E-04 mol/(m^2*s).

$$J_{H_2} = C_g * m * k_l$$

(13)

Where
- J_{H2} is the flux of hydrogen gas into the liquid phase [mol/(m^2*s)]

- C_g is the concentration of the gas phase [mol/m^3]
- m is the equilibrium constant
- K_l is the mass transfer coefficient for the liquid interface [m/s]

When you divide the obtained flux by the surface of the interface layer between the gas and the liquid phase [0.05 m^2], a rate is obtained of 5E-06 mol/s. With the rate and the calculated dissolved molar mass of hydrogen in the groundwater volume inside the keykeg®, the time required to reach equilibrium is estimated to be around 99 min for with a partial pressure of 3 bar hydrogen.

8.2 Appendix B: PHREEQC model

TITLE Aquifer towards equilibrium

SELECTED_OUTPUT 1
   -file   H2_zaltbommel.txt
   -simulation   false
   -state   false
   -solution   false
   -distance   false
   -time   false
   -temperature   true
   -alkalinity   true
   -totals   C(-4) Ca Cl K Mg Mn Na
               P S(-2) S(6) Fe(2) Fe(3) H0
       Si Zn Pb Ba
   -equilibrium_phases Quartz Goethite Siderite Pyrite
             Hematite Fe(OH)3(a) Magnetite Calcite
   -saturation_indices CO2(g) H2(g) H2S(g) CH4(g)
             Goethite Siderite Pyrite Hematite
             Fe(OH)3(a) Magnetite Calcite
   -gases   CO2(g) H2(g) H2S(g) CH4(g)

########### Solution 1: Groundwater composition (Depending on location of groundwater ##########

SOLUTION 1
   temp   18
   pH   6.96
   pe   4
   redox   pe
   units   mmol/L
   density 1
   Alkalinity 2.796
   Ca   2.170
   Cl   0.71
   Fe   0.179
   K   0.026
   Mg   0.398
   Mn   0.016
   Na   1.746
   P   0.031
   S   0.472
   Si 0.585
   -water   1 # kg

REACTION_PRESSURE 1
3.5

REACTION_TEMPERATURE 1

15

```
EQUILIBRIUM_PHASES 1
   Quartz        0.0   1.17
   Calcite       0.0   0.5
   #Goethite        0.0   0
   Siderite      0.5   0.1
   #Pyrite       0.0   0
   #Hematite        0.0   0
   #Fe(OH)3(a)      0.0   0
   #Magnetite       0.0   0

GAS_PHASE 1
   fixed_pressure
   pressure 3.5
   volume 0.36
   temperature 15
   CH4(g)    0
   CO2(g)    0.01
   H2(g)     0
   H2S(g)    0

EXCHANGE 1   ## mol/kg
   X      0.00026
   Y      0.0000325
   Z      0.0000325
   -e     1

SAVE SOLUTION 2
SAVE GAS_PHASE 2
SAVE EQUILIBRIUM_PHASES 2

END

TITLE Leakage of hydrogen

USE SOLUTION 2
USE GAS_PHASE 2
USE EQUILIBRIUM_PHASES 2

REACTION_PRESSURE 1
3.5

REACTION_TEMPERATURE 1
14.9

REACTION 1
   H2(g)    1
   3 millimoles in 13 steps

INCREMENTAL_REACTIONS true
```

```
SAVE SOLUTION 3
SAVE GAS_PHASE 3
SAVE EQUILIBRIUM_PHASES 3

END
```

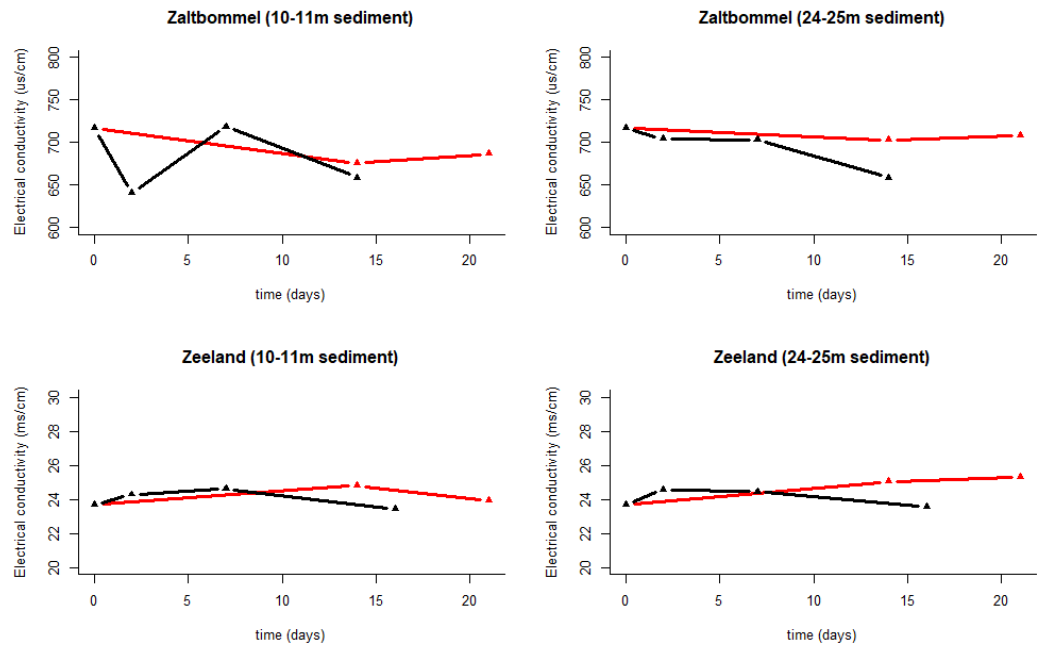## 8.3 Appendix C: Other experimental results

Figure 24: Electrical conductivity plotted against time for the reference incubations (red) and the incubations with added hydrogen (black)
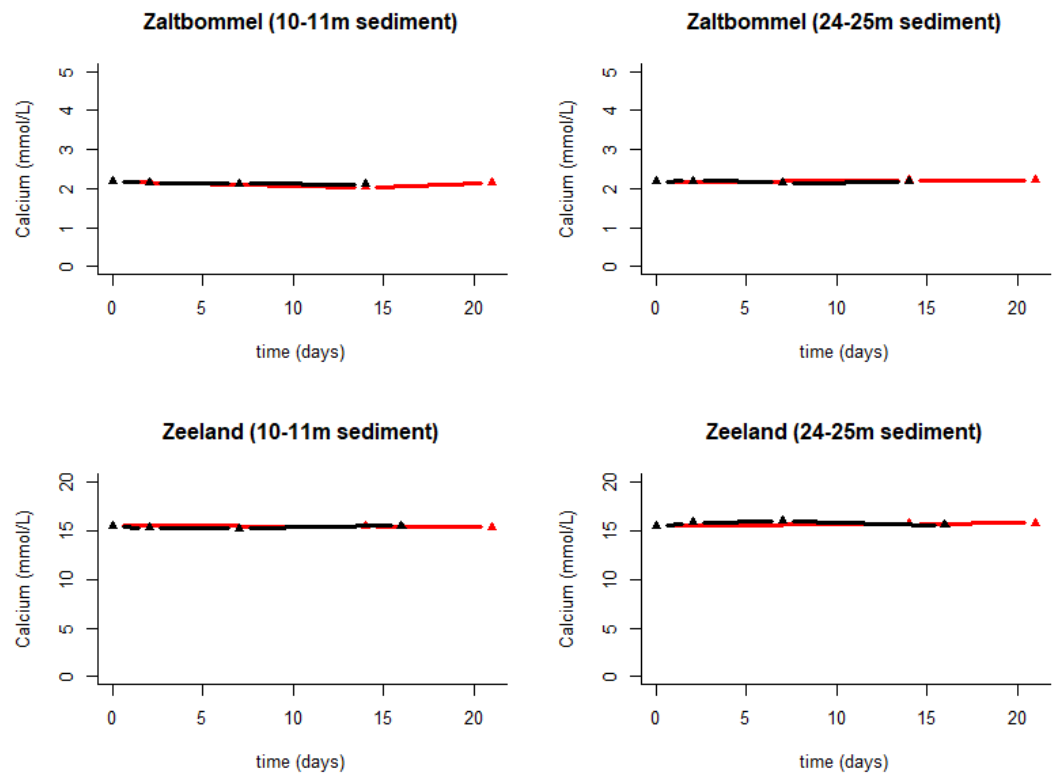
Figure 25: Calcium concentration plotted against time for the reference incubations (red) and the incubations with added hydrogen (black)
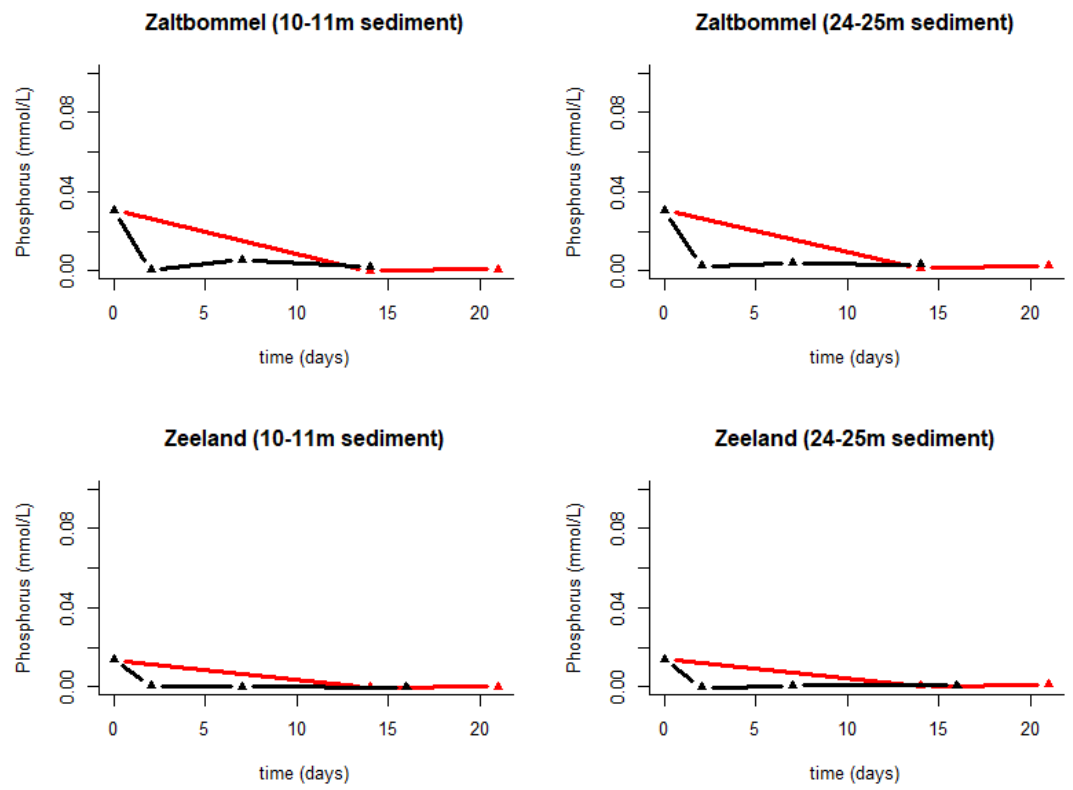
Figure 26:   Phosphorus concentration plotted against time for the reference incubations (red) and the incubations with added hydrogen (black)
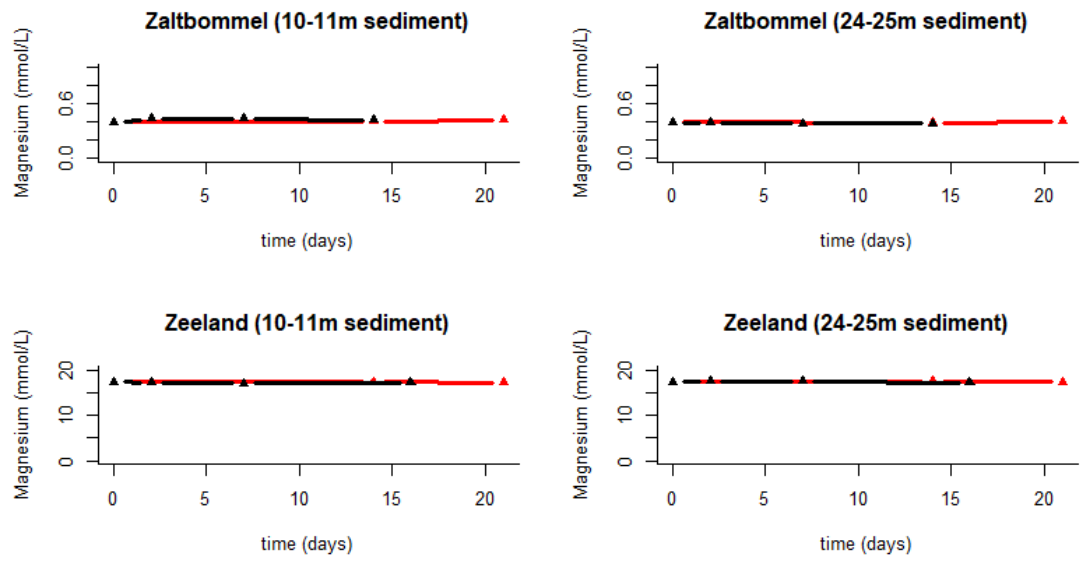
Figure 27:　Magnesium concentration plotted against time for the reference incubations (red) and the incubations with added hydrogen (black)

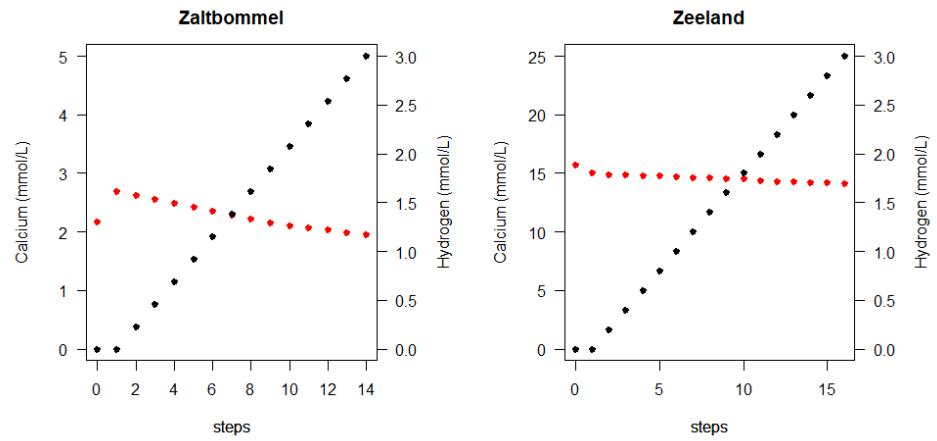## 8.4　　　Appendix D: Other modelling results

Figure 28: The equilibrium between the concentration of calcium (left axis, red) and hydrogen (right axis, black) for each step of hydrogen addition in the model
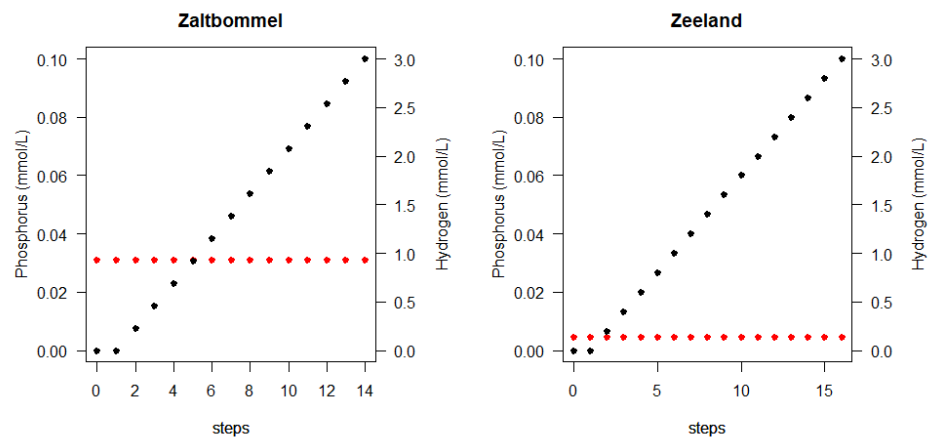
Figure 29: The equilibrium between the concentration of phosphorus (left axis, red) and hydrogen (right axis, black) for each step of hydrogen addition in the model